Clays and Clay Minerals, Vol. 51, No. 3, 231–251, 2003.

GEOCHEMICAL SIGNATURES OF PALEODEPOSITIONAL AND DIAGENETIC ENVIRONMENTS: A STEM/AEM STUDY OF AUTHIGENIC CLAY MINERALS FROM AN ARID RIFT BASIN, OLDUVAI GORGE, TANZANIA

VICTORIA C. HOVER[1,*] AND GAIL M. ASHLEY[2]

[1] Department of Earth and Environmental Science, Rutgers University, Newark, NJ 07081-1819, USA
[2] Department of Geological Sciences Rutgers University, Piscataway, NJ 08854-8066, USA

Abstract—Olduvai Gorge, Tanzania (East African Rift) exposes a 100 m thick Plio-Pleistocene sequence of dominantly volcaniclastic sediments deposited in a 50 km wide closed basin containing a playa lake. A scanning transmission electron and analytical electron microscopy (STEM/AEM) study of authigenic clay minerals in sediments from representative depositional environments in the basin (pyroclastic fan, fluvial plain, wetland, lake margin and lake basin) was undertaken to determine whether clay compositions and textures could provide unique geochemical fingerprints characteristic of source area (Plio-Pleistocene trachytic volcanics *vs*. Precambrian quartzose-feldspathic basement) or paleoenvironmental conditions.

Our study shows that compositional signatures obtained by clay minerals during early pedogenesis are inherited from their parent source rocks. Sediments sourced from volcanics contain highly disordered, dioctahedral smectite. Those sourced from Precambrian basement are similar, but are more Al-rich. Subsequent neoformation in the pedogenic (soil) or diagenetic (lake-margin, lake) environments results in the modification of original clay mineralogy, compositions, and textures, and unique paleoenvironmental fingerprints are acquired. Soils developed on the distal pyroclastic fan contain smectite with more Fe(III) and Mg than smectite from the proximal pyroclastic fan sediments. A trend of decreasing Al and increasing Mg content occurs in smectite compositions in samples from the fluvial to lake-margin and lake environments as a result of partial replacement of original dioctahedral Al-rich smectite by neoformed trioctahedral Mg-rich smectite (stevensite). Neoformed celadonite replaces smectite in the most saline lake sediments.

The STEM/AEM data collectively indicate that diagenesis in the saline-alkaline lake results in the replacement of Al-rich dioctahedral smectite by Mg-rich trioctahedral smectite (stevensite) and Mg- and Al-rich celadonite. Thus, determination of clay mineral compositions at a basin-wide scale provides a useful tool for interpreting the spatial distribution of depositional and diagenetic environments.

Key Words—Celadonite, Clay Neoformation, Early Diagenesis, Pedogenesis, Smectite.

INTRODUCTION

Reconstruction and interpretation of ancient sedimentary environments provides information on climate, provenance, weathering and transport of sediment, as well as subsequent diagenesis (Reading, 1996). Continental rift systems are well-documented archives of thick sedimentary sequences that comprise depositional environments containing sediments ranging from coarse-grained alluvial fan to fine-grained lacustrine deposits (Frostick *et al.*, 1986; Ashley and Renaut, 2002). Fine-grained sediments, however, are often difficult to interpret because they lack physical structures (bedding, ripples, *etc.*) or visible minerals. Fossils are particularly rare in arid continental settings and thus, clay minerals become an important record of the paleoenvironments or the paleoclimate. Continental rift systems also commonly contain volcaniclastic sediments containing highly reactive glass fragments (ash, pumice). Rapid alteration of volcanic glass to clay minerals usually takes place soon after deposition (*e.g.* Fiore, 1993). Continued *in situ* alteration of these neoformed clays in the pedogenic environment and subsequent erosion and transport into other depositional environments may result in further diagenetic alteration in response to changing water compositions.

With the growing interest in future climate change, one of the first steps in understanding the Earth's complex climate system is to understand past climate. Authigenic clay minerals are likely to be sensitive indicators of the geochemical environment of deposition and diagenesis. Thus, the spatial and temporal distribution of authigenic clay minerals in continental settings becomes an important record of paleoenivronmental and paleoclimatic conditions (*e.g.* Singer, 1980, 1984; Webster and Jones, 1994). There is a need to know to what extent clay mineral neoformation is a robust record of environmental conditions in ancient settings. But the fine-grained nature of clay minerals and slow reaction rates in arid settings make interpretation of clay mineral geochemistry difficult. What portion of the textural or compositional signature is inherited from the parent source rocks? What are the textural or geochemical fingerprints acquired in the depositional environment? How are the original clay minerals altered in the

* E-mail address of corresponding author:
vhover@andromeda.rutge rs.edu
DOI: 10.1346/CCMN.2003.0510301

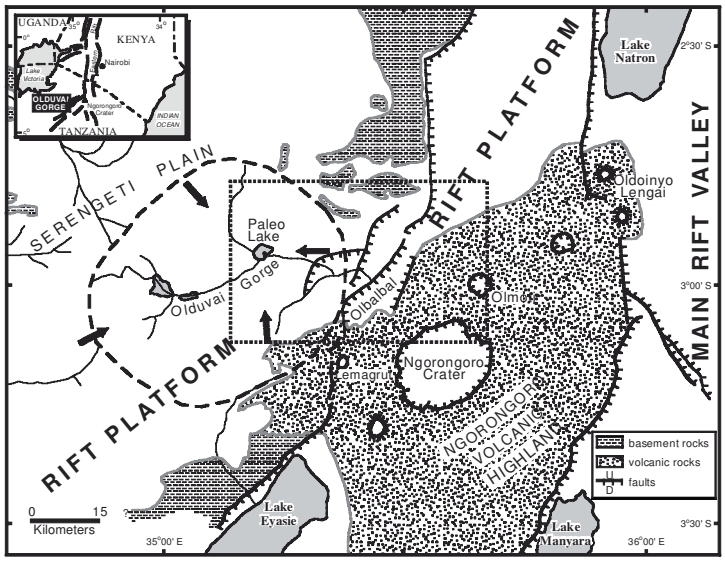

Figure 1. Olduvai Gorge is located in northern Tanzania (inset map) just west of the Ngorongoro Volcanic Highland, which straddles the East African Rift valley. The main East African Rift Valley is to the east of the Gorge and the Serengeti Plain to the west. The approximate location of the paleobasin (~50 km diameter) is indicated by the dashed line. Arrows represent directions of sediment flux into the basin (from Ashley and Hay, 2002). The study area (rectangle) is enlarged in Figure 2.

pedogenic or diagenetic environment? In short, how do you tell the difference between original detrital and authigenic clays? In order to tease apart the complex detrital *vs.* authigenic signatures in clay minerals at the nanometer scale, we applied STEM/AEM techniques to study clay minerals from various depositional environments in the paleo-Olduvai basin, a small (50 km wide) sedimentary basin located on the margin of the main East African rift valley (Figures 1,2).

Recent paleoanthropologically-directed fieldwork at Olduvai Gorge in arid East Africa reconstructed the paleo-landscape of the Olduvai basin during a narrow window of time (a 100 ky 'time slice') beginning at ~1.85 Ma (Figure 3a). The time slice is near the base of a 2 my sedimentary record containing extensive vertebrate (including hominids) and cultural remains of central importance in the study of human evolution (Leakey, L.S.B., 1965; Leakey, M.D., 1971; Kappelman, 1984, 1986; Hay, 1990; Blumenschine and Masao, 1991; Peters and Blumenschine, 1995; Blumenschine and Peters, 1998). One hundred and three archaeological excavations (trenches) placed by the Olduvai Landscape Paleoanthropology Project (OLAPP) within an East–West transect across the basin yielded a high-resolution

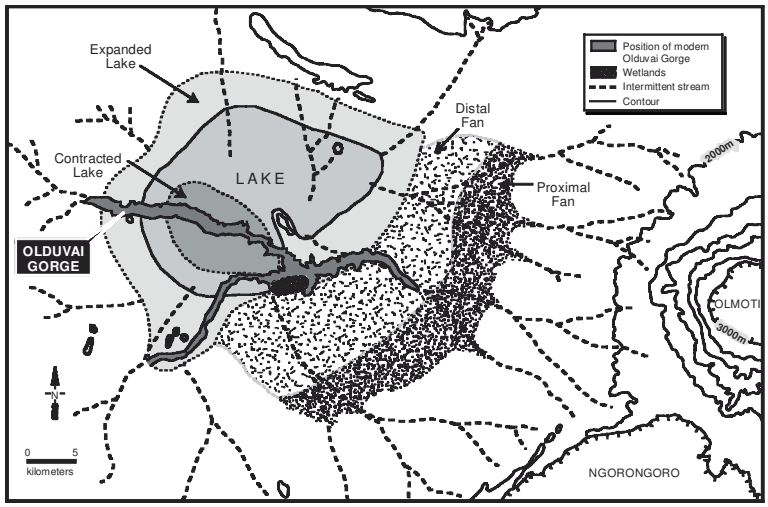

Figure 2. A diagrammatic reconstruction of the study area as it existed during the early Pleistocene (~1.75 Ma). Ephemeral streams drained off the Ngorongoro Volcanic Highland from the east and south. A playa lake in the basin center expanded and contracted through time. A groundwater-fed wetland was located southeast of the lake. Rivers transporting quartzose-feldspathic sediment drained into the basin from west and north (After Ashley and Hay, 2002).

https://doi.org/10.1346/CCMN.2003.0510301 Published online by Cambridge University Press

stratigraphy containing a variety of lithologic facies. Thus, the site is ideal for the investigation of possible links between depositional environments and clay mineralogy because the source material, the physical setting and paleoenvironmental conditions are reasonably well known (Hay, 1976; Ashley and Hay, 2002).

Previous investigations by Hay and Kyser (2001) have shown that Mg-rich smectitic clays and celadonite are the principal diagenetic clay minerals in the saline-alkaline lake environment of the Olduvai basin. Deocampo *et al.* (2002) used clay mineral compositions within a local area of the lake-margin and wetlands to separate saline from freshwater deposits. These studies were based on analysis of bulk clay-mineral separates and did not include a detailed examination of other depositional environments, such as the pyroclastic alluvial fan, fluvial plain, or paleosols. Studies of modern continental saline alkaline lakes have also documented that neoformation of Mg-rich smectite and 10 Å illite-like clay takes place in lake-basin sediments (*e.g.* Stoffers and Singer, 1979; Singer and Stoffers, 1980; Yuretich and Cerling, 1983; Jones and Weir, 1983; Jones, 1986). These studies were also based on analysis of bulk clay-mineral separates and did not include other depositional environments. Banfield *et al.* (1991b) used TEM methods to characterize Mg-smectite neoformation in the saline-alkaline Lake Abert, Oregon, but no diagenetic 10 Å illitic or celadonitic phase was observed in those sediments.

The objectives of our study were to use XRD and STEM/AEM techniques to (1) characterize the clay mineralogy of sediments from a variety of lithologies along a transect across the paleo-sedimentary Olduvai basin; (2) determine the textural and geochemical fingerprints acquired during early weathering to see whether the clay minerals retain any compositional signatures from the parent source rocks; and (3) determine the extent to which these early signatures are modified by more extensive pedogenesis or post-depositional diagenetic alteration. To our knowledge, this is the first high-resolution STEM/AEM study to document the progressive diagenetic reaction of smectite to celadonite in a saline alkaline lake setting.

PHYSICAL SETTING

Geology

The Olduvai Gorge is located 3° south of the equator in northern Tanzania (Figure 1). The Gorge was formed during mid-to-late Pleistocene time when the Olduvai River incised through a 100 m thick, 2 my old stack of interbedded tephras and reworked pyroclastic sediments. These deposits accumulated in a shallow, ~50 km wide basin situated on the margin of the East African Rift between quartzose-feldspathic Precambrian shield rocks (west) and Plio-Pleistocene trachytic volcanic highlands (east) (Hay, 1976) (Figure 2). The thickness of sediments within the narrow 100 ky time slice decreases with distance from the Ngorongoro Volcanic Highland source area, from ~8 m in the east to ~4 m in the lake basin. The thickness increases to 6 to 8 m in the fluvial plain deposits sourced mainly from the Serengeti Plain to the west.

Paleoenvironments and Sedimentology

The relief of the paleolandscape was ~1500 m (Figure 3). Volcanic eruptions produced an episodic rain of pyroclastic ejecta that created a pyroclastic fan adjacent to the volcanic highland in the east. A paucity of well-developed fluvial channels, as well as the presence of freshwater wetland deposits suggest that there was little surface drainage and that water was in the subsurface seeping out at the lake margin (Figure 3c) (Liutkus and Ashley, in press). The distal fan area was a low-gradient undulating surface comprising fine-grained tuffaceous claystones. There is widespread evidence for pedogenesis on the distal fan suggesting intense weathering and a fluctuating groundwater table in an alkaline environment (Ashley and Driese, 2000).

The topography on the western fluvial plain was a low-relief surface with broad (100 m wide) and shallow intermittent streams carrying quartzose-feldspathic bedload (Ashley and Hay, 2002). The broad interfluves were composed of tuffaceous claystones presumably reworked and transported by wind from volcanic sources on the east side of the lake (Figure 3c) (Ashley and Hay, 2002).

The Olduvai basin was closed and contained a small saline-alkaline playa lake that expanded and contracted (probably driven by wet/dry cycles) over a broad lake-margin flat (Hay, 1976; Ashley, 2001; Ashley and Hay, 2002) (Figures 2,3a). Waxy claystones are the geologic record of the lake at high stages and the earthy claystones the record of a groundwater-fed wetland that developed at low-lake stages (Ashley, 1996; Liutkus and Ashley, in press; Ashley and Driese, 2000). The presence of Magadi-type chert nodules and carbonate pseudomorphs after evaporite minerals in the waxy claystones suggest high salinity and pH (9.5–10) conditions as a result of evapo-concentration at this equatorial site (Hay and Kyser, 2001). The alteration of volcanic glass and detrital clays occurred rapidly in the alkaline-saline lake water resulting in the formation of authigenic Mg-rich smectite, celadonite, zeolites and K-feldspar (*e.g.* Hay, 1970, 1976; Hay and Kyser, 2001).

In summary, the sediments vary systematically from primary volcaniclastics in the east to physically reworked and chemically altered (*i.e.* highly weathered) volcaniclastics in the west. There are five distinct lithofacies: silty lapilli-rich claystone, silty tuffaceous claystone, tuffaceous claystone, earthy claystone, and waxy claystone (*e.g.* Ashley and Hay, 2002). Table 1 summarizes the characteristics and environment of deposition of each facies.

https://doi.org/10.1346/CCMN.2003.0510301 Published online by Cambridge University Press

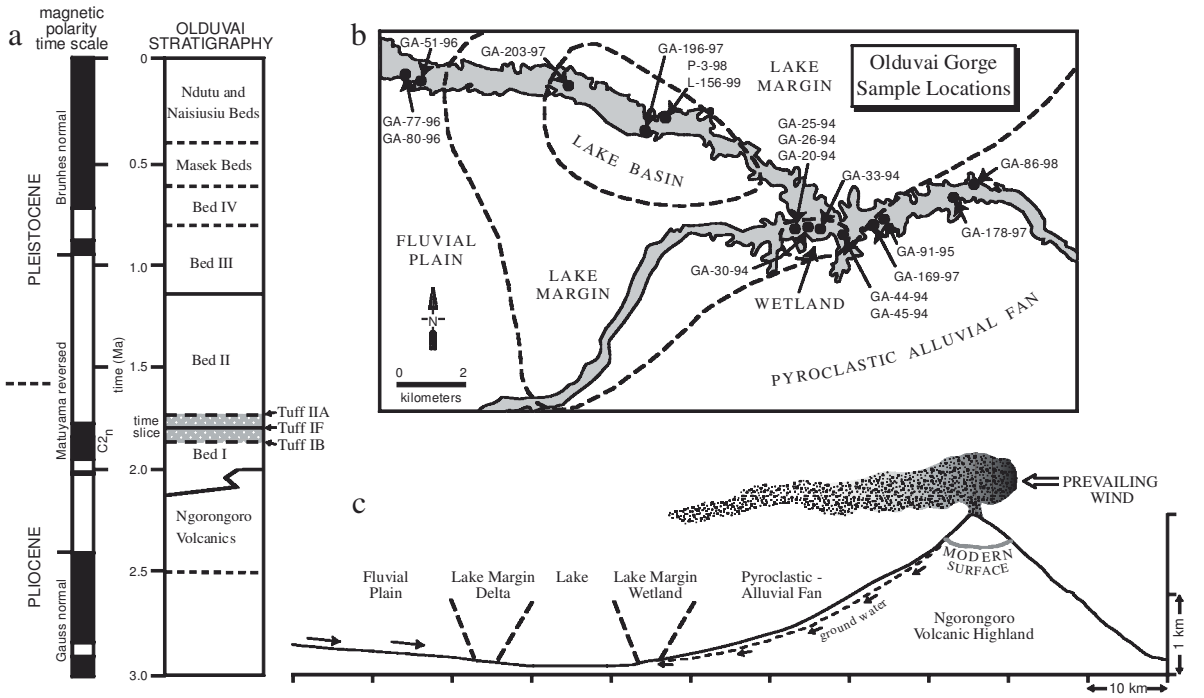

Figure 3. (a) The Olduvai basin stratigraphic section is related to the late Pliocene-Pleistocene magnetic timescale (normal polarity in black, reversed in white). The samples studied in detail were taken from the 100 ky time slice from upper Bed I and lowermost Bed II sediments between Tuffs IB and IIA. (b) 18 samples representing each depositional environment (proximal and distal fan, wetland, lake margin, lake basin, and fluvial plain) were chosen for sampling along a 20 km transect across the central portion of the paleobasin. (c) A schematic topographic cross-section depicts the location of depositional environments. Prevailing eastern trade winds transported primary pyroclastic material and reworked volcaniclastic sediments westward (after Ashley and Hay, 2002).

Table 1. Lithologies, associated depositional environments and stratigraphic positions of samples.

Lithology	Characteristics, mineralogy	Depositional environment	Hay locality	Stratigraphic positions	Sample numbers
Silty, lapilli-rich claystone	Pumice and lapilli of trachyte composition; K-feldspar, plagioclase feldspar, zeolites	Proximal pyroclastic fan	6 31	UBI LMBII	GA-86-98 GA-178-97
Silty tuffaceous claystone	Silt-sized volcanic minerals, minor lapilli; K-feldspar, plagioclase feldspar, trace mica, no zeolites	Fluvial plain	66 66a 66a	UBI UBI UBI	GA-51-96 GA-77-96 GA-80-96
Tuffaceous claystone	Light brown to reddish brown ash-sized pyroclasts (mineral crystals, glass, lithics), soil features; K-feldspar, plagioclase feldspar, zeolites	Distal pyroclastic fan; lake-margin flats	34 35	LMBII LMBII	GA-91-95 GA-169-97
Earthy claystone	Earthy luster, beige, siliceous phytoliths, diatoms, plant fossils; detrital? feldspars, authigenic calcite, trona	Freshwater wetlands	85 43 39	LMBII LMBII LMBII	GA-25-94 GA-30-94 GA-44-94
Waxy claystone	Waxy luster, green/gray; K-feldspar (authigenic?), and authigenic zeolites, Mg-rich smectite	Lake margin	85 85 42a 39	LMBII LMBII LMBII LMBII	GA-20-94 GA-26-94 GA-33-94 GA-45-94
	Waxy luster, green/gray; authigenic calcite, K-feldspar, zeolites, Mg-rich smectite, and celadonite	Lake basin	54 49 80 80	LMBII LMBII LMBII LMBII	GA-203-97 GA-196-97 L-156-99 P-3-98

UBI = upper Bed I
LMBII = lowermost Bed II

https://doi.org/10.1346/CCMN.2003.0510301 Published online by Cambridge University Press

METHODOLOGY

Field

Over 100 archaeological step trenches (3–8 m deep and 1–2 m wide) were excavated in early Pleistocene upper Bed I and lowermost Bed II sediments between Tuffs IB and IIA (100 ky 'time slice') (Figure 3a). The excavations were logged for lithology, fossils, sedimentary structures, and artifacts. Eighteen sediment samples from 12 sites representing the major lithologies in each depositional environment within the basin were chosen for detailed clay mineral analysis (Table 1, Figure 3b).

Laboratory

Sediment mineralogy. X-ray diffraction (XRD) analyses of homogenized bulk samples were obtained on acetone smears of hand-ground material. Oriented clay-separate aggregates (<2 μm) were obtained by centrifugation of bulk material in distilled water (*e.g.* Jackson, 1969), filtered (<0.45 μm), and transferred to a glass slide (Drever, 1973). The XRD analyses were obtained on air-dried and ethylene glycol-saturated clay aggregates (General Electric XRD-5 diffractometer, 40 kV and 20 mA, Ni-filtered CuKα radiation, scintillation detector, 1° entrance slit and 0.2° receiving slit). Digital strip-charts were obtained (2° min^{-1}) and peak positions determined manually.

STEM/AEM microanalyses. Clay-sized material from each sample was examined by STEM/AEM methods (Philips CM12, 120 kV, beam current ~20 μA, University of Michigan). Two procedures were used to prepare samples (Peacor, 1992a): (1) clay separates were dispersed in isopropyl alcohol and collected on lacy C-coated Cu grids to obtain grain mounts of clay particles with **c*** parallel to the electron beam; (2) globules of mud were impregnated in L.R. White Resin (Kim *et al.*, 1995) from which ion-milled samples of clay particles were obtained with **c*** perpendicular to the electron beam. The TEM imaging, SAED patterns and AEM analyses were obtained using instrument conditions, standards, and analysis of spectra as described by Jiang *et al.* (1990) and Hover *et al.* (2002). Lattice-fringe images were obtained, using mainly over-focus (~100 nm) conditions to maximize contrast related to compositional differences (*e.g.* Guthrie and Veblen, 1990). The SAED patterns were obtained over an area of ~200 nm^2 (770 mm camera length, 10 μm aperture).

The AEM analyses (Kevex Quantum system) were obtained in the scanning mode using a 50 Å diameter spot rastered over 50 nm^2. Examination of the TEM images shows that even at this fine resolution, the analyses may result from a mixture of several individual crystallites. Great care was taken to obtain analyses in the same areas where lattice-fringe images and SAED patterns indicated relatively homogeneous, clay-rich material. Approximately 10 spot analyses were obtained from each sample. The AEM cation ratios were normalized to the $O_{20}(OH)_4$ unit-cell cations per formula unit (c.p.f.u.) (Laird, 1994) assuming all Fe as Fe(III). Care was taken to minimize diffusional loss of alkalis (*e.g.* van der Pluijm *et al.*, 1988) by incorporating the entire grain in the area of the rastered beam. All Mg was assigned to octahedral sites, though it is possible that some Mg^{2+} may be in the interlayers. Estimated uncertainties in the atomic proportions of Si and Al are ~±0.1 c.p.f.u.; of Fe(III), Mg, Ti and Ca, ~±0.05 c.p.f.u.; of K, ~±0.2 c.p.f.u.; and of Na, ~0.3 c.p.f.u. (*e.g.* Peacor, 1992b; Warren and Ransom, 1992). The Na atomic proportions are particularly suspect due to high background levels at low X-ray energies, and the possible presence of NaCl or Na carbonates from evaporated soil moisture. Incorporation of volcanic glass or amorphous silica gel coatings in the area of analyses was possible, but evident as excess Si and Na. These analyses were discarded.

RESULTS

Pyroclastic fan and fluvial plain

Clay mineralogy. The XRD pattern of the <2 μm clay-aggregate fraction from tuffaceous claystones from the proximal pyroclastic fan (Figure 4a) is representative of both the pyroclastic fan and fluvial plain environments. The pattern is dominated by smectite-rich clay with basal 001 spacings of ~12.7–13.9 Å in air-dried samples, which expand to ~17.2–17.3 Å in the glycol-solvated samples. The presence of weak higher-order 00*l* reflections at ~8.58–8.67 Å and ~5.54-5.62 Å indicate that up to ~20% randomly interstratified illite may be present in the smectite (Reynolds, 1980; Moore and Reynolds, 1997). Similar smectite-rich XRD patterns were obtained for the <2 μm clay-aggregate fraction from paleosols developed in the tuffaceous claystones on the distal pyroclastic fan. Some paleosol XRD patterns also contain weak reflections at ~10.1 Å indicating that a trace amount of discrete 10 Å illite-like phase is also present (not shown).

Texture/structure. The TEM images show that the alteration of volcanic glass fragments (ash and pumice) to smectite-rich clay minerals is pervasive in the tuffaceous claystones of the pyroclastic fan and fluvial plain. Commonly, corroded volcanic glass particles are coated by small (~20–50 nm diameter) crystallites, some with subhedral pseudohexagonal grain boundaries (Figure 5a). The SAED patterns of such material (Figure 5b) contain diffuse *hk*0 rings characteristic of highly disordered, turbostratic stacking of smectite 00*l* layers with random rotations about **c*** (*e.g.* Peacor, 1992a). The pattern may also result from superposition of several smectite crystallites with disordered interfaces between them.

https://doi.org/10.1346/CCMN.2003.0510301 Published online by Cambridge University Press

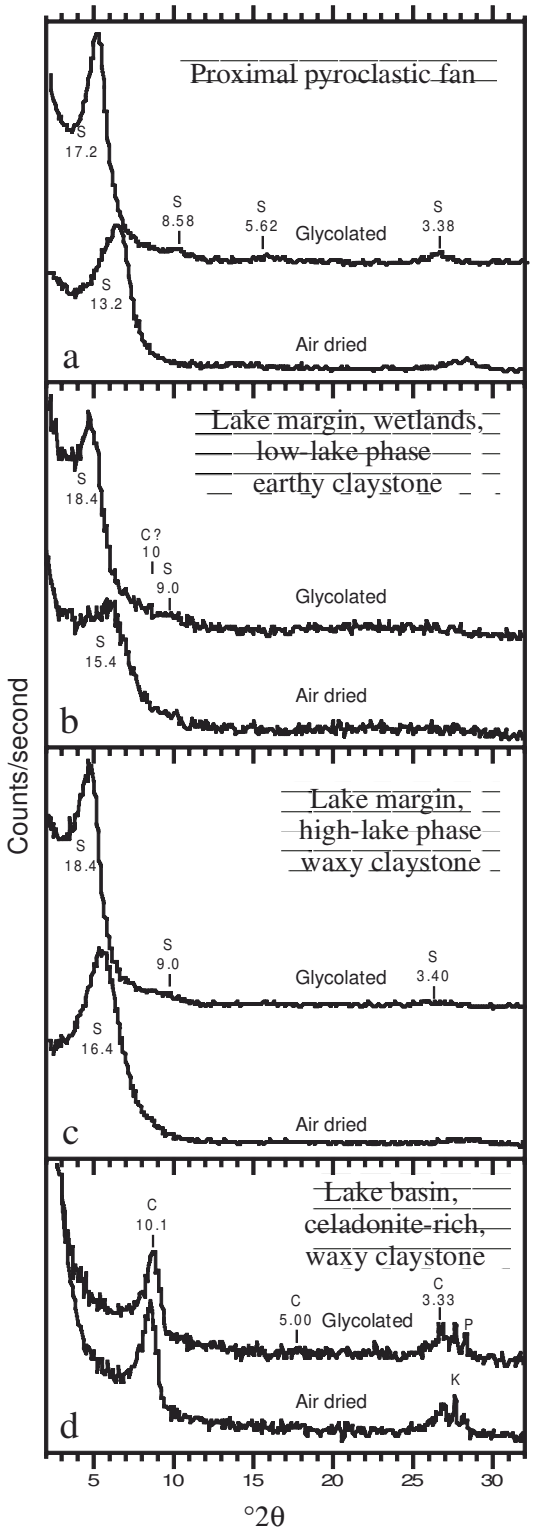

Figure 4. XRD patterns of <2 μm clay aggregates from (a) a tuffaceous claystone from the proximal pyroclastic fan containing mostly smectite (GA-178-97), (b) an earthy claystone from the lake margin containing smectite (GA-44-94), (c) a waxy claystone from the lake margin containing smectite (GA-26-94), and (d) a waxy claystone containing 10 Å clay (GA-196-97).

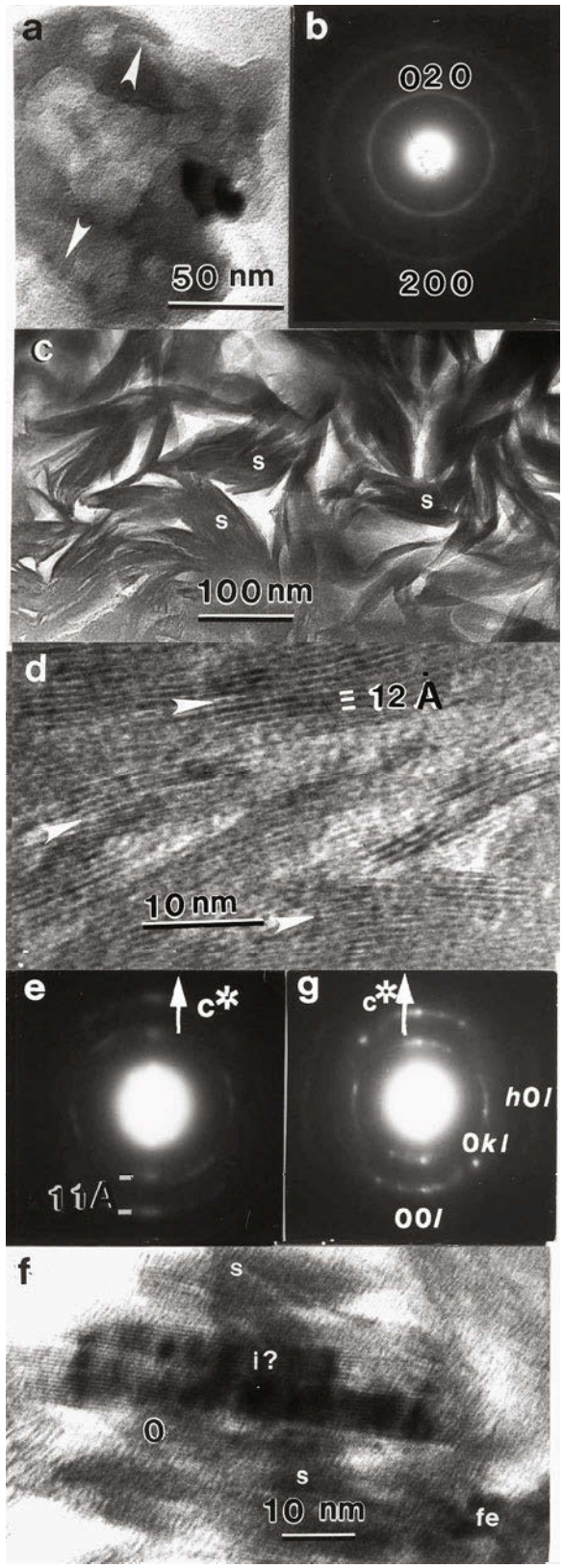

Figure 5. (Caption on facing page.)

https://doi.org/10.1346/CCMN.2003.0510301 Published online by Cambridge University Press

In ion-thinned samples, the clay alteration of glass particles appears as an anastomosing feathery intergrowth of wispy crystallites (Figure 5c). At high magnification, crystallites oriented with **c*** perpendicular to the electron beam display wavy 001 lattice fringes with *d* values ranging from 11 to 12 Å and many layer terminations and other defects characteristic of smectite (Figure 5d). Individual crystallites commonly have curved shapes and are only a few layers thick (~3 to 5 nm) and <~50 nm long. Several adjacent crystallites, with low-angle interfaces between them form larger aggregates of subparallel grains up to ~20 layers thick (~20 nm) and up to ~100 nm long. Only small areas of the aggregates are in proper orientations to show clear lattice-fringe images indicating highly disordered stacking of crystallites (Figure 5d).

The SAED patterns of such intergrowths contain reflections resulting from a mixture of several disordered crystallites (Figure 5e). The 00*l* reflections are diffuse parallel to **c*** consistent with the variable smectite basal spacings of >10 Å (Peacor, 1992a; Dong and Peacor, 1996). The fanning of diffraction spots perpendicular to **c*** is consistent with the subparallel nature of the smectite crystallites within larger aggregates. The presence of both *h*0*l* and 0*kl* reflections (*e.g.* 01*l* or 02*l* and their pseudohexagonal equivalents (*e.g.* 11*l* or 22*l* for which $k \neq 3N$) and the diffuseness parallel to **c*** indicate that the stacking of smectite layers about **c*** is disordered (turbostratic). The superposition of *hk*0 diffraction rings in the SAED pattern results from the physical mixture of some crystallites oriented with **c*** parallel to the electron beam as in grain mount samples.

The TEM images of clay mineral alteration in paleosols developed on the distal pyroclastic are generally similar to those described for the proximal pyroclastic fan. However, in addition to smectite, characterized by its thin packet size, and irregular 001 lattice-fringe images (~10.5 to 11 Å interlayer spacing), there are larger packets that have relatively straight lattice-fringe images with more regular 001 basal spacings (~10 Å) (Figure 5f). The SAED patterns obtained on such material have better-developed 00*l* and 0k*l* reflections containing discrete spots consistent with the presence of some $1M_d$ polytypism, which is characteristic of illite-like material (*e.g.* Baxter Grubb *et al.*, 1991; Peacor, 1992a). Diffuseness parallel to **c*** indicates that disordered smectite-like layers are also present within the area of the SAED pattern (Figure 5g). The paleosol samples also contain Fe oxyhydroxides, which occur as small clusters of extremely small (<5 nm), relatively equant particles. The Fe oxyhydroxides do not appear to have any structural relationship with the associated smectite (*i.e.* topotactic intergrowth or exsolution features).

Composition. Representative calculated structural formulae obtained from AEM spot analyses of smectite from tuffaceous claystones of the proximal pyroclastic fan are similar to those of the western fluvial plain within the error of the analyses. Total octahedral occupancies are Al-rich and dominantly dioctahedral, containing ~4 cations per $O_{20}(OH)_4$ formula units (c.p.f.u.) (Table 2). Substitution of Al for tetrahedral Si and Mg for octahedral trivalent cations results in net negative interlayer charges of ~–0.9 to –1.7 c.p.f.u.. The tetrahedral charge is generally <50% indicating that compositions are dominantly montmorillonitic (octahedral layer-charge deficient). The net negative interlayer charge is balanced primarily by interlayer Na (0.6 to 1.1 c.p.f.u.) and K (0.1 to 0.6 c.p.f.u.). Sodium is the dominant interlayer cation in all analyses.

The proportions of octahedral ^{vi}Al, Mg and Fe(III) in smectite samples from the proximal pyroclastic fan (Figure 6a) are compared to those obtained in smectite from the fluvial plain (Figure 6b). The Al contents are >~45 mol.%, and Mg and Fe(III) contents are about equal at ~25 to 30 mol.%. The average octahedral cation proportions of smectite from the western fluvial plain are slightly more Al-rich (^{vi}Al:Mg:Fe(III) = 56:23:21 mol.% (n = 38)) and more homogeneous than smectite from the pyroclastic fan (^{vi}Al:Mg:Fe(III) = 52:25:23 mol.% (n = 28)). The compositions of smectite from the paleosol horizons developed in the distal pyroclastic fan tend to have a higher proportion of octahedral Mg and Fe(III) relative to ^{vi}Al than smectite from the proximal pyroclastic fan or fluvial plain (*e.g.* average ^{vi}Al:Mg:Fe(III) = 45:29:26 mol.% (n = 22)) (Figure 6c).

Lake margin and wetlands

Clay mineralogy. Along the eastern margin of the lake, waxy claystones deposited during periods of lake

Figure 5 (*facing page, RH column*). TEM images and SAED patterns of samples from the pyroclastic fan. (a) TEM image of a corroded clay-size glass (ash) fragment from the proximal pyroclastic fan coated by smectite crystallites (arrows) (grain mount sample, GA-86-98). (b) SAED pattern of smectite shown in (a) contains diffuse *hk*0 rings consistent with turbostratic stacking of smectite layers. The inner ring corresponds to 020 reflections and their symmetrical equivalents (~4.6 Å) and the second ring to 200 reflections and their symmetrical equivalents (~2.6 Å). (c) Low magnification TEM image of smectite (s) alteration of volcanic glass fragment (clear areas) from the proximal pyroclastic fan (ion-thinned sample, GA-178-97). (d) High magnification TEM image of (c) showing thin smectite crystallites with wavy lattice fringes, variable interplanar spacings, and layer terminations and dislocations (arrows). (e) The SAED image of smectite shown in (d) contains diffuse 00*l* reflections in the **c*** direction and both *h*0*l* and 0*kl* consistent with turbostratic stacking of layers. (f) TEM image of 10 Å illite (i?) in a paleosol developed on the distal pyroclastic fan. Smectite (s) and Fe oxyhydroxides (fe) are also present (ion-thinned sample, GA-91-95). (g) SAED pattern of illite-rich area shown in (f) containing discrete 0*kl* reflections consistent with $1M_d$ polytypism.

https://doi.org/10.1346/CCMN.2003.0510301 Published online by Cambridge University Press

Table 2. Structural formulae of smectite-rich clay: western fluvial plain and pyroclastic fan.

Paleodepositional environment	Proximal pyroclastic fan	Proximal pyroclastic fan	Western fluvial plain	Western fluvial plain	Western fluvial plain	Distal pyroclastic fan, paleosol	Distal pyroclastic fan, paleosol
Sample number	GA-86-98 IM	GA-178-97 IM	GA-77-96 GM	GA-80-96 IM	GA-51-96 IM	GA-91-95 IM	GA-169-97 GM
Hay locality	6	31	66a	66a	66	34	35
Structural formula							
Si	7.48	7.61	7.56	7.78	7.35	7.50	7.60
^{iv}Al	0.52	0.39	0.44	0.22	0.65	0.50	0.40
Tetrahedral charge	−0.52	−0.39	−0.44	−0.22	−0.65	−0.50	−0.40
^{vi}Al	2.63	2.28	1.97	2.66	2.13	1.93	2.07
$Fe^{3+\dagger}$	0.64	0.71	0.87	0.45	0.92	0.77	0.72
Mg	0.71	0.96	1.12	0.87	0.93	1.26	1.24
Mn	0.00	0.03	0.00	0.00	0.03	0.00	0.05
Ti	0.07	0.07	0.00	0.05	0.00	0.10	0.07
Octahedral occupancy	4.05	4.05	3.96	4.02	4.01	4.06	4.15
Octahedral charge	−0.52	−0.76	−1.24	−0.76	−0.92	−0.98	−0.78
Na	0.88	0.59	1.08	0.76	1.07	0.96	0.92
K	0.14	0.29	0.60	0.14	0.50	0.40	0.25
Ca	0.00	0.14	0.00	0.04	0.00	0.06	0.00
Interlayer charge	1.02	1.15	1.68	0.96	1.57	1.48	1.18
Tetrahedral charge %	51.0	33.9	26.2	22.4	41.4	33.8	33.9
Mg/(^{iv}Al+Fe^{3+}+Mg) %	17.8	24.3	28.2	21.9	23.4	32.0	30.7

† All Fe calculated as Fe^{3+}
GM = grain mount sample; IM = ion-milled sample

expansion are interbedded with earthy claystones deposited during periods of lake contraction, when groundwater-fed springs created a freshwater wetland (Ashley, 2000; Liutkus and Ashley, 2003; Ashley and Hay, 2002). The XRD patterns of <2 μm glycol-solvated clay aggregates from the lake-margin earthy and waxy claystones are similar. Both are dominated by very poorly crystalline and/or fine-grained smectite, with broad d_{001} reflections at 15.4–16.4 Å in the air-dried samples that expand to 17.9–19 Å in the glycol-solvated samples (Figure 5c). Weak 002 reflections occur between 8.84 and 9.30 Å, at rational subdivisions of the d_{001} value. Higher-order 00*l* reflections are poorly developed in the earthy claystone samples, though weak 005 reflections at 3.35–3.38 Å are present in some waxy claystone samples (Figure 5c).

Liutkus (2000), Hay and Keyser (2001) and Deocampo *et al.* (2002) interpreted d_{001} values of >~17 Å, and non-rational *d* values of higher-order 00*l* reflections to result from interstratification of illite. However, extremely thin particles (<~10 nm) may also produce the observed XRD patterns in the glycol-solvated samples, which causes 001 and 002 peaks to shift to lower 2θ, but does not affect the positions of the 003 or higher-order peaks (R.C. Reynolds, 2002, pers. comm.).

Texture/structure. The TEM images of ion-thinned samples of the earthy claystones show that relict volcanic glass particles are commonly altered to wispy feathery smectite intergrowths with crystal morphologies, packet size, and degree of ordering similar to that observed in smectite from the proximal pyroclastic fan or fluvial plain (Figure 7a). However, some areas of the altered glass contain larger smectite aggregates composed of tens of individual crystallites only a few layers thick, which are stacked in a sub-parallel arrangement with low-angle interfaces between them to form highly disordered 'quasi'-crystals (Figure 7b). The individual crystallites have irregular interplanar spacings of 11–12 Å, many layer terminations, and other defects. The SAED pattern of such material shows diffuse 00*l* reflections with spacing >10 Å and the presence of both 0*kl* and *h*0*l* consistent with turbostratic stacking of layers (Figure 7c).

Smectite alteration of glass particles from lake-margin waxy claystones is generally similar to that observed in the earthy claystones (Figure 7d). However, smectite 'quasi-crystals' are commonly larger in the waxy claystones relative to the earthy claystones (Figure 7e). Lattice-fringe images of the 'quasi'-crystals show individual domains with interlayer spacings ranging from 11 to 14 Å (Figure 7e). The smaller basal spacings are characteristic of smectite. The larger 14 Å spacings may indicate the presence of hydroxide groups in the interlayer. The SAED patterns obtained on such material have diffuse 00*l*, 0*kl* and *h*0*l* reflections parallel

https://doi.org/10.1346/CCMN.2003.0510301 Published online by Cambridge University Press

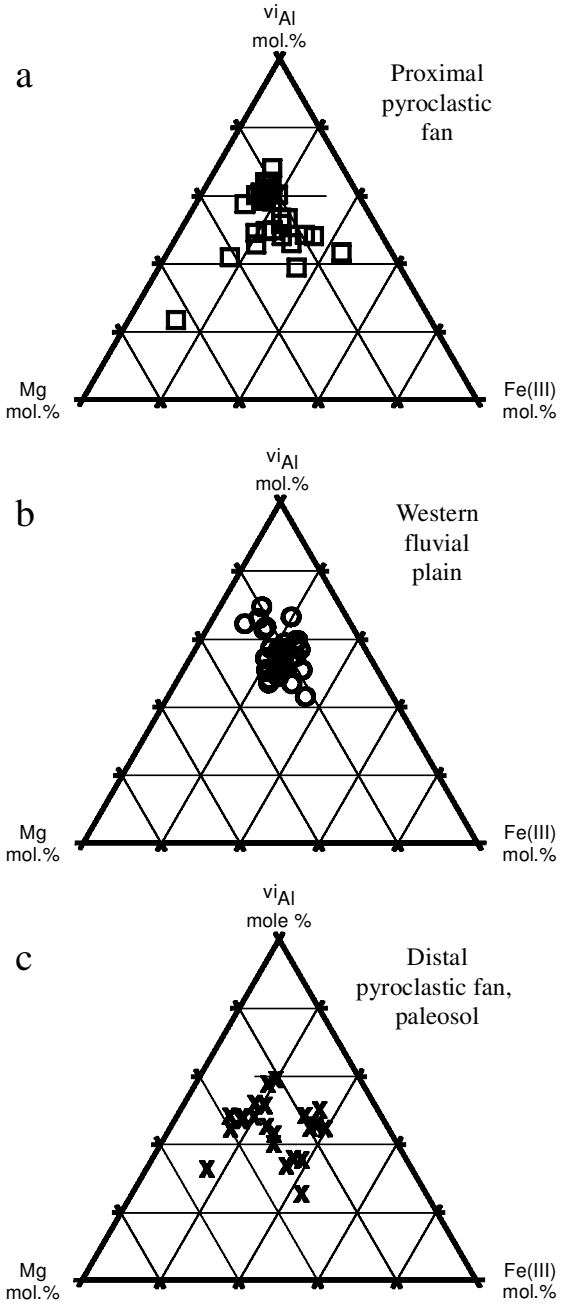

Figure 6. The octahedral cation proportions of (a) smectite from the proximal pyroclastic fan (average ^{vi}Al:Mg:Fe(III) = 52:25:23 mol.% (n = 28)); (b) smectite from the western fluvial plain, (average ^{vi}Al:Mg:Fe(III) = 56:23:21 mol.% (n = 38)); and (c) smectite from well developed paleosols on the distal pyroclastic fan (average ^{vi}Al:Mg:Fe(III) = 45:29:26 mol.% (n = 22)).

to **c*** and are consistent with disordered turbostratic stacking of smectite-like layers (Figure 7f).

The TEM images of waxy claystones also show evidence for the formation of an authigenic phyllosilicate. In a grain mount sample of a waxy claystone oriented such that **c*** is parallel to the electron beam, a cluster of small crystallites <30 nm in diameter display sub- to euhedral pseudohexagonal grain boundaries consistent with neoformation (Figure 7g). The SAED pattern of this aggregate contains diffuse rings with embedded discrete spots, groups of which can be related by pseudohexagonal symmetry (*e.g.* 60º rotation about **c*** (Figure 7h). The discrete diffraction spots are consistent with the presence of individual smectite crystallites composed of coherent stacks of layers (*e.g.* MacEwan crystallites), several of which are related to each other by random rotations about the **c*** axis.

The TEM images of ion-thinned samples also show that within most smectite-rich aggregates described above there are small domains (<10 layers thick and 20–30 nm long) with relatively straight and uniform 10 Å lattice fringes, consistent with the presence of illite-like material (Figure 7i). No interstratification with 10 Å illite-like layers was observed within the smectite domains, rather discrete crystallites composed of smectite-like and illite-like layers were observed. The SAED patterns obtained from these areas have diffuse 00*l* reflections parallel to **c*** and both 0*kl* and *h*0*l* reflections consistent with turbostratic stacking in smectite-like layers (Figure 7j). Embedded within the diffuse 0*kl* reflections are some discrete spots, which are smeared in the **c*** direction, indicating that some $1M_d$ polytypism may be present (Figure 7j). These reflections may result from the incorporation of some of the 10 Å illite-like (celadonite?) clay material within the field of the SAED pattern.

Composition. The composition of smectite from the earthy claystones varies from dominantly Al-rich dioctahedral compositions similar to smectite from the proximal pyroclastic fan to more Mg-rich compositions similar to smectite from the waxy claystones described below. Representative structural formulae of low-Mg (<1 c.p.f.u.) and high-Mg (>2 c.p.f.u.) analyses are given in Table 3. The low-Mg analysis has an octahedral occupancy of <4.2 c.p.f.u., though the high-Mg analyses have octahedral occupancies up to 4.4 c.p.f.u. indicating the presence of mixed di- and trioctahedral components. The total interlayer charge of ~–1.5 to –1.9 c.p.f.u. is higher than observed in samples from the pyroclastic fan and fluvial plain, and largely balanced by higher Na contents (0.9 to 1.4 c.p.f.u.). Some of the high Na values are probably due to the incorporation of a small amount of secondary Na carbonate within the area of analysis.

Smectite compositions from the lake-margin waxy claystones are generally more Mg-rich than smectite compositions obtained from interbedded earthy claystones (Table 3). Relatively low-Mg compositions are generally dioctahedral (Table 3), but, high-Mg compositions (>2.5 c.p.f.u.) have octahedral sheet occupancies up to 4.8 c.p.f.u. indicating that a substantial trioctahedral component is present. The relatively low

https://doi.org/10.1346/CCMN.2003.0510301 Published online by Cambridge University Press

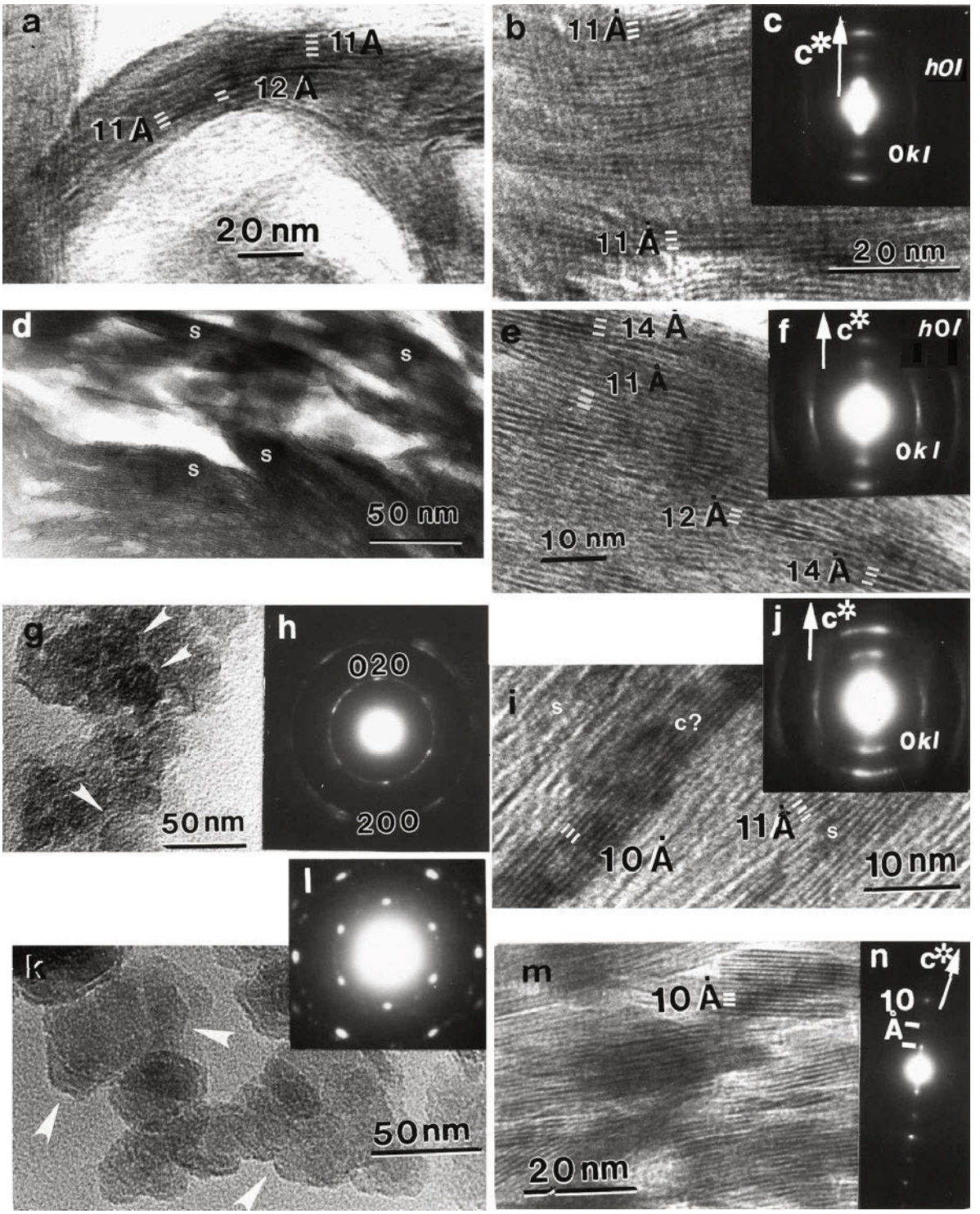

Figure 7. TEM images and SAED patterns of lake margin and basin samples. (a) TEM image of smectite alteration in an earthy claystone from the wetlands environment (ion-thinned sample, GA-44-94). (b) High-magnification TEM image of an earthy claystone showing several thin (<10 nm) subparallel smectite crystallites with wavy and irregular 001 lattice fringes and highly disordered interfaces between crystallites (ion-thinned sample, GA-44-94). (c) SAED pattern of smectite shown in (b) contains diffuse 00*l* reflections in the **c*** direction and both *h*0*l* and 0*kl* consistent with disordered turbostratic stacking of layers. (d) Low-magnification TEM image of smectite (s) alteration of volcanic glass fragment in a lake-margin waxy claystone (ion-thinned sample, GA-26-94). (e) High-magnification TEM image of an Mg-rich smectite 'quasi-crystal' enlarged from (d) composed of

https://doi.org/10.1346/CCMN.2003.0510301 Published online by Cambridge University Press

tetrahedral charge and octahedral charge deficiency indicates that the compositions are similar to the Mg- and Si-rich stevensite (*e.g.* Faust and Murata, 1953; Brindley, 1955; Faust *et al.*, 1959), rather than saponite. Total interlayer charges of ~ –1.1 to –1.7 c.p.f.u. and Na contents (0.8–1.4 c.p.f.u.) are similar to the smectite compositions in the earthy claystones.

The proportions of octahedral ^{vi}Al:Mg:Fe(III) in smectite analyses from the earthy claystones (Figure 8a) show that the proportion of ^{vi}Al varies from compositions similar to those observed in smectite from the pyroclastic fan (^{vi}Al:Mg:Fe(III) = 62:19:19 mol.%) to moderately Mg-rich compositions (^{vi}Al:Mg:Fe(III) = 26:52:22 mol.%) (Figure 8a) (average ^{vi}Al:Mg:Fe(III) = 40:37:23 mol.% (n = 25)). The compositions of the most Mg-poor smectite from the waxy claystones (^{vi}Al:Mg:Fe(III) = 43:39:19 mol.%) overlap compositions from the earthy claystones, but extend to compositions with higher Mg proportions (*e.g.* ^{vi}Al:Mg:Fe(III) = 5:82:13 mol.%) consistent with an increase in a trioctahedral Mg-rich component (Figure 8b) (average ^{vi}Al:Mg:Fe(III) = 20:61:19 mol.% (n = 37)).

Lake basin

Clay mineralogy. Sediments in the central basin are characterized by waxy claystones with various proportions of smectite-rich and 10 Å-rich clay as major constituents. The XRD pattern of a <2 μm clay-aggregate fraction of a waxy claystone containing mostly 10 Å clay shows a sharp diffraction peak at 10.1 Å, which does not shift upon glycol solvation. Higher-order 00*l* reflections corresponding to ~5.0 Å and 3.33 Å are consistent with 10 Å-clay material. K-feldspar and plagioclase feldspar are also present in most clay fraction samples. The XRD patterns of smectite in lake-basin waxy claystones are similar to those for the lake-margin waxy claystones.

Texture/structure. A TEM image of a clay-separate grain-mount of a waxy claystone containing mostly 10 Å clay shows very fine-grained euhedral crystallites (<~30 nm diameter) with pseudohexagonal grain boundaries (Figure 7k). The SAED pattern of these crystallites has discrete *hk*0 spots with hexanet symmetry consistent with coherent stacking of layers (*e.g.* MacEwan crystallites) (Fig 7l). Minor smearing of diffraction spots into diffuse rings suggests the possibility of some disordered interfaces between coherent layers (*e.g.* smectite-like layers), or the superposition of multiple grains, with slight differences in orientation about **c***.

The TEM images of crystallites oriented with **c*** perpendicular to the electron beam show relatively straight 001 lattice fringes with 10 Å spacing (Figure 7m). Individual crystallites consist of packets of from ~10–15 layers (~10–15 nm) and are <~30 nm in length. Some layer terminations and other defects are present at the interfaces between grains. The crystallites cluster to form aggregates with low-angle interfaces (Figure 7m). The SAED pattern of the crystallites shows sharp 00*l* reflections with ~10 Å spacing (Figure 7n). The 0*kl* reflections also contain some discrete spots with smearing parallel to **c*** consistent with 1M_d polytypism.

Composition. Smectite analyses of samples from the lake basin are the most Mg rich analyzed and are consistent with stevensite compositions. Representative mineral formulae contain up to ~5 c.p.f.u. with total octahedral occupancies of 5.3 to 5.4 c.p.f.u. consistent with mainly trioctahedral compositions (Table 3). Total interlayer charges of ~ –0.9 to –1.0 c.p.f.u. are balanced primarily by Na (0.5–0.7 c.p.f.u.), and small amounts of K (~0.1 c.p.f.u.) and Ca (~0.1 c.p.f.u.). The maximum octahedral Mg content is ~95 mol.% and the combined proportions of ^{vi}Al and Fe(III) are <10 mol.% (Figure 9c) (average ^{vi}Al:Mg:Fe(III) = 4:90:6 mol.% (n = 7).

Analyses of the 10 Å clay mineral in waxy claystones from the lake margin and lake basin indicate that compositions are dioctahedral, and Si rich, consistent with celadonite (*e.g.* Seifert, 1968; Odin, 1988) (Table 4). Sample GA-196-97 contains the most celadonitic material. The Mg content is ~2 c.p.f.u., and the Al and Fe(III) contents are ~1 c.p.f.u. each. The total interlayer charge of ~ –1.7 to –2.0 c.p.f.u. is higher than observed for smectite-rich clays and K is the dominant interlayer cation instead of Na (Table 4). The average

several thin subparallel smectite crystallites with disordered interfaces between them and variable 001 interplanar spacings. (f) SAED pattern of smectite shown in (e) contains diffuse 00*l* reflections in the **c*** direction and both *h*0*l* and 0*kl* reflections consistent with disordered turbostratic stacking of layers. (g) TEM image of an aggregate of discrete crystallites with pseudohexagonal grain boundaries (arrows) (grain mount sample, GA-20-94). (h) SAED pattern contains discrete reflections, sets of which can be related by 60° rotations about **c***, indicating the presence of several coherent (MacEwan) crystallites. These reflections are superimposed on diffuse *hk*0 rings indicating that some turbostratic smectite layers are also present. (i) TEM image of 10 Å clay mineral (c?) with relatively straight and uniform lattice fringes and celadonitic composition within a smectite-rich (s) quasi-crystal. (j) SAED pattern of celadonite-rich area of (j) with discrete 0*kl* reflections consistent with 1M_d polytypism. (k) Low-magnification TEM image of an aggregate of celadonite crystallites from a waxy claystone in the lake basin with euhedral pseudohexagonal grain boundaries (arrows) (grain mount sample, L-156-99). (l) SAED pattern of celadonite in (j) displaying discrete hexanet reflections consistent with coherent (MacEwan) crystallites. (m) High-magnification TEM image of celadonite showing individual crystallites are only ~10–15 nm thick and ~30–50 nm long. Lattice fringes are relatively straight and have uniform 10 Å interplanar spacings (ion-thinned sample L-156-99). (n) SAED pattern of celadonite contains sharp 00*l* reflections consistent with uniform 10 Å interplanar spacings.

https://doi.org/10.1346/CCMN.2003.0510301 Published online by Cambridge University Press

Table 3. Structural formulae of smectite-rich clay: lake margin and lake basin.

Paleodepositional environment	Lake margin, wetlands, earthy claystone	Lake margin, wetlands, earthy claystone	Lake margin, wetlands, earthy claystone	Lake margin, wetlands, earthy claystone	Lake margin, waxy claystone	Lake margin, waxy claystone	Lake margin, waxy claystone	Lake margin, waxy claystone	Lake margin, waxy claystone	Lake margin, waxy claystone	Lake basin, waxy claystone	Lake basin, waxy claystone
Sample number	GA-44-94 IM	GA-44-94 IM	GA-30-94 GM	GA-25-94 GM	GA-45-97 GM	GA-33-97 GM	GA-26-94 IM	GA-26-94 IM	GA-20-94 IM	GA-20-94 GM	P-3-98 IM	P-3-98 IM
Mg content	Low Mg	High Mg	High Mg	High Mg	Low Mg	High Mg	High Mg	High Mg	High Mg	High Mg	High Mg	High Mg
Hay locality	39	39	43	85	39	42a	85	85	85	85	80	80
Structural formula												
Si	7.66	7.56	7.67	7.77	7.89	7.58	7.89	7.76	7.75	7.59	7.93	7.96
^{iv}Al	0.34	0.44	0.36	0.23	0.11	0.42	0.11	0.24	0.25	0.41	0.07	0.04
Tetrahedral charge	−0.34	−0.44	−0.33	−0.23	−0.11	−0.42	−0.11	−0.24	−0.25	−0.41	−0.07	−0.04
^{vi}Al	2.33	1.15	1.36	1.05	1.94	0.66	0.70	0.30	0.83	0.33	0.13	0.17
$Fe^{3+\dagger}$	0.72	0.95	0.60	0.88	0.61	0.71	0.59	0.57	0.72	0.50	0.25	0.25
Mg	0.70	2.08	2.38	2.07	1.43	3.04	3.31	3.72	2.60	3.53	5.02	4.86
Mn	0.00	0.03	0.07	0.06	0.06	0.07	0.00	0.10	0.02	0.09	0.00	0.00
Ti	0.05	0.06	0.00	0.08	0.08	0.12	0.07	0.13	0.10	0.17	0.00	0.00
Octahedral occupancy	3.80	4.28	4.41	4.14	4.11	4.59	4.68	4.82	4.27	4.62	5.40	5.29
Octahedral charge	−1.23	−1.21	−1.21	−1.64	−1.0	−1.20	−1.21	−1.22	−1.72	−1.0	−0.83	−1.00
Na	1.35	1.33	0.83	1.24	0.76	1.10	0.90	0.92	1.35	0.95	0.51	0.69
K	0.22	0.31	0.45	0.64	0.14	0.42	0.42	0.34	0.62	1.04	0.11	0.14
Ca	0.00	0.00	0.13	0.00	0.14	0.05	0.00	0.10	0.00	0.00	0.14	0.11
Interlayer charge	1.57	1.64	1.53	1.87	1.18	1.62	1.32	1.46	1.97	1.99	0.90	1.04
Tetrahedral charge %	21.7	26.8	21.6	39.1	9.4	25.9	8.3	16.4	12.7	20.6	7.8	3.8
Mg/(^{iv}Al+Fe^{3+}+Mg) %	18.7	49.7	54.8	52.0	35.8	68.9	71.9	81.1	62.7	81.0	93.0	92.0

† All Fe calculated as Fe^{3+}

GM = grain mount sample; IM = ion-milled sample

Table 4. Structural formulae of celadonite-rich clay: lake margin and lake basin.

Paleodepositional environment	Lake margin, waxy claystone	Lake basin, waxy claystone	Lake basin, waxy claystone	Lake basin, waxy claystone	Lake Basin, waxy claystone	Lake Basin, waxy claystone
Sample number	GA-26-94 IM	GA-203-97 IM	GA-196-97 IM	GA-196-97 IM	L-156-99 IM	P-3-98 IM
Hay locality	85	54	49	49	80	80
Structural formula						
Si	7.52	7.86	7.85	7.82	7.77	7.52
^{iv}Al	0.48	0.11	0.15	0.18	0.23	0.48
Tetrahedral charge	−0.48	−0.11	−0.15	−0.18	−0.23	−0.48
^{vi}Al	1.04	1.26	1.09	1.04	0.30	1.01
$Fe^{3+\dagger}$	0.87	0.95	1.00	0.95	0.99	0.80
Mg	2.22	2.53	1.98	2.07	3.02	2.29
Mn	0.15	0.00	0.00	0.00	0.08	0.00
Ti	0.09	0.00	0.07	0.07	0.07	0.12
Octahedral occupancy	4.36	4.43	4.14	4.13	4.45	4.2
Octahedral charge	−1.19	−1.24	−1.50	−1.61	−1.66	−1.52
Na	0.73	0.42	0.63	0.84	0.46	0.60
K	0.94	0.96	1.01	0.96	1.43	1.12
Ca	0.00	0.00	0.00	0.00	0.00	0.14
Interlayer charge	1.67	1.38	1.65	1.80	1.89	2.00
Tetrahedral charge %	28.7	10.2	9.2	10.0	14.3	24.0
Mg/(^{iv}Al+Fe^{3+}+Mg) %	53.7	57.2	43.4	50.9	70.7	55.9

† All Fe calculated as Fe^{3+}
GM = grain mount sample; IM = ion-milled sample

^{vi}Al:Mg:Fe(III) ratio of sample GA-196-97 is 26:47:27 mol.% (n = 8) (Figure 9c). The other analyses of celadonite-rich material reported in Table 4 generally contain more Mg and total octahedral occupancies are >4.2 c.p.f.u.. These compositions probably reflect mixtures with Mg-rich smectite material within the area of the analyses.

DISCUSSION

Smectite and illite neoformation – pedogenic (weathering) environment

Early pedogenic smectite neoformation. The alteration of silt- to clay-size volcanic glass particles (ash, pumice) to smectite-rich clay in the poorly developed soils of the proximal pyroclastic fan and fluvial plain is pervasive. The overall similarity in clay mineralogy in these two widely spaced environments is consistent with the westward eolian transport of volcanic ash and pumice from the Ngorongoro volcanic centers (Hay, 1976; Ashley and Driese, 2000; Hay and Kyser, 2001; Ashley and Hay, 2002) (Figure 3) and the subsequent alteration of the volcaniclastic material in both environments under similar subaereal pedogenic conditions. The surface-water geochemistry at the time of alteration was probably dominated by Na^{+}-HCO_3^{-}-CO_3^{2-}-rich compositions and alkaline pH largely controlled by weathering of the sodic trachytic volcanic rocks (*e.g.* Garrels and Mackenzie, 1967) and carbonatite volcanism (Hay, 1970, 1976, 1989).

The TEM images of the altered glassy particles in the poorly developed soils of the proximal pyroclastic fan and fluvial plain indicates that smectite textures are consistent with early stages of neoformation. The smectite alteration consists of anastomosing, feathery intergrowths of many very small crystallites (<~5 nm thick, < ~50 nm long) (Figure 5c) with highly disordered interfaces between them (Figure 5d). Individual crystallites have wavy and irregular 001 lattice-fringe images (11–13 Å) consistent with expanded smectite layers, which are turbostratically stacked about **c*** (Figure 5e). Similar textures and disordered structures have been produced in hydrothermal alteration experiments using natural and synthetic glass (*e.g.* de la Fuente *et al.*, 2000) and have been observed in volcanic glass, ash and pumice particles altered in the near-surface environment (Tazaki *et al.*, 1989; Banfield *et al.*, 1991a; Fiore, 1993; Banfield and Barker, 1998).

The AEM analyses of smectite from the proximal fan and fluvial fan are also consistent with neoformation in the weathering environment. Sodium is the dominant interlayer cation (Table 2), which is consistent with both the Na-rich content of the original volcanic glass and of the soil moisture during weathering. Potassium also makes up a significant fraction of the interlayer cations. The total interlayer charge is >1.5 c.p.f.u. in ~40% of the spot analyses obtained on smectite from these samples. Such high interlayer charges are usually attributed to the presence of interstratified illite-like layers (*e.g.* Środoń

https://doi.org/10.1346/CCMN.2003.0510301 Published online by Cambridge University Press

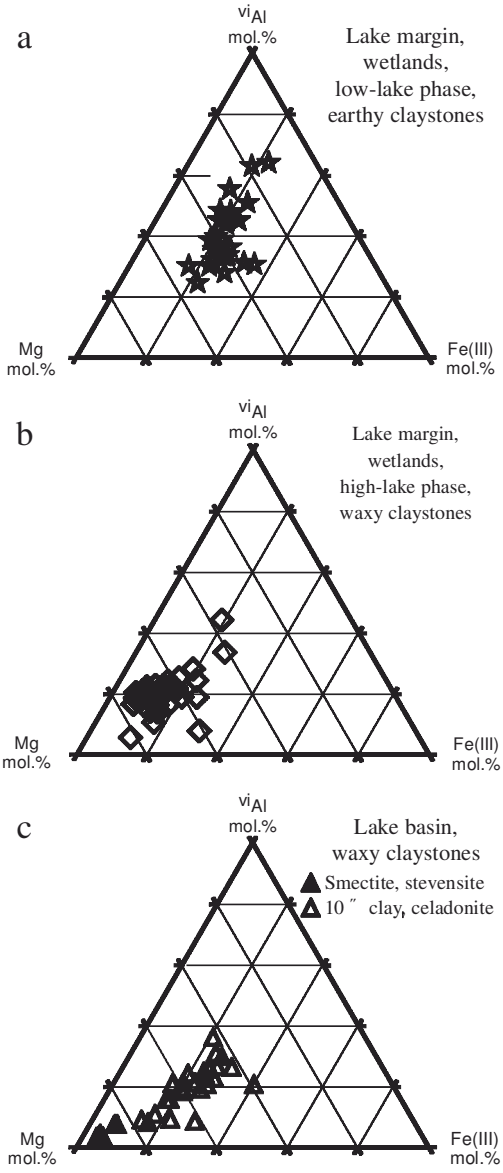

Figure 8. The octahedral cation proportions of (a) smectite from earthy claystones, wetlands lake margin (low-lake phase) (average ^{vi}Al:Mg:Fe(III) = 40:37:23 mol.% (n = 25)); (b) smectite from waxy claystones, lake margin (high-lake phase) (average viAl:Mg:Fe(III) = 20:61:19 mol.% (n = 37)); (c) smectite and celadonite in waxy claystones from the lake basin (average ^{vi}Al:Mg:Fe(III) = 4:90:6 mol.% (n = 7) and 22:57:21 mol.% (n = 24), respectively).

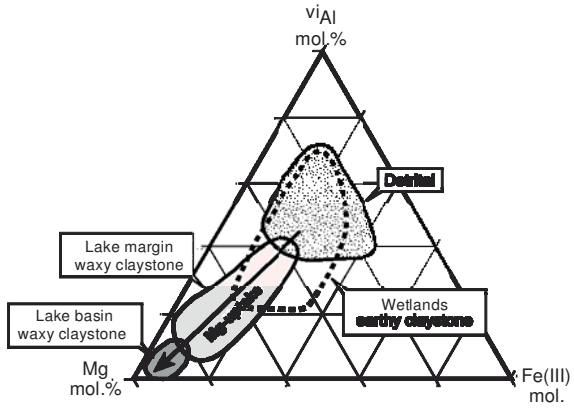

Figure 9. Basin-wide geochemical trends in the octahedral cation proportions of ^{vi}Al:Mg:Fe(III) in smectite.

et al., 1986). However, our TEM images showed no direct evidence for interstratification of smectite with illite-like 10 Å layers, using over-focus conditions (*e.g.* Guthrie and Veblen, 1990). Alternatively, under the conditions of repeated wetting and drying common to pedogenic environments, smectite may also preferentially take up K (Eberl *et al.*, 1986). However, because the individual crystallites are so thin, the presence of illite-like layers may not be easily detected in TEM images (*e.g.* Banfield *et al.*, 1991a) and we cannot rule out the possibility that some interstratified illite-like layers may be present in the smectite.

The dominantly Al-rich, dioctahedral compositions of smectite from both the proximal pyroclastic fan and fluvial plain sediments are consistent with a common source and early pedogenic conditions influenced by relatively uniform solute chemistry. The average octahedral ^{vi}Al:Mg:Fe(III) proportions of smectite from the fluvial plain samples are slightly more Al rich indicating a possible contribution from the weathering of feldspars derived from the quartzose-feldspathic basement rocks. However, within the error of analyses, the variations in smectite compositions from each environment are insignificant (Figure 6a,b). These Al-rich dioctahedral compositions of early pedogenic smectites from both environments represent the original 'detrital' clay component (Figure 9).

Pedogenic illite neoformation. The smectite alteration of volcanic glass in the well developed soils from the distal pyroclastic fan is generally similar to that observed in the poorly developed soils. However, there are subtle textural, mineralogical and compositional changes, which indicate that there is a higher degree of pedogenic alteration. The TEM images of smectite-rich intergrowths in the paleosols often contain scattered domains of more-ordered material characterized by thicker crystallites (~10–15 nm) with relatively straight 001 lattice-fringe images and uniform (~10 Å) basal spacings consistent with illite-like material (Figure 5f). The SAED patterns contain some discrete 0kl diffraction spots, which implies some degree of coherency (ordering) between layers and reflections are smeared parallel to **c***, consistent with 1M_d polytypism (*e.g.* Peacor, 1992a) (Figure 5g).

These textural observations are consistent with the relatively high K contents and interlayer charges of >1.5 c.p.f.u. in >50% of the spot analyses obtained from the well developed soils. The preferential uptake of K in

https://doi.org/10.1346/CCMN.2003.0510301 Published online by Cambridge University Press

smectite interlayers during repeated wetting and drying cycles has been shown to cause adjacent smectite layers to become oriented to one another by rational 60° rotations about **c*** (instead of random turbostratic rotations) and the collapse of smectite interlayers to ~10 Å as in illite (*e.g.* Eberl *et al.*, 1986).

Most of the AEM analyses of smectite from the well developed paleosols are Al-rich and dominantly dioctahedral. However, several of the analyses plot at higher Mg and Fe(III) contents than smectites from the proximal fan and fluvial plain (Figure 6c). The increase in the K, Mg and Fe(III) contents, the increase in the interlayer charge, and the subtle increase in degree of ordering between smectite interlayers suggests that additional smectite neoformation took place in these deeply weathered paleosols. Thus, our microtextural and microgeochemical observations are consistent with the bulk geochemical results of Ashley and Driese (2000), which indicated that smectite neoformation must be taking place to account for the observed increase in K in the bulk sediment relative to likely parent materials. The presence of more abundant analcime in these paleosols also indicates that soil solutions were probably influenced by more alkaline pore fluids than the proximal pyroclastic fan. These fluids were probably introduced during periodic inundation by the alkaline lake (Ashley and Driese, 2000).

Mg-smectite and celadonite neoformation—lake margin and lake environments

The Al-rich dioctahedral smectite particles formed in pedogenic environments and transported by eolian or fluvial processes provided the reactive detrital clay source-material for subsequent diagenetic alteration in the wetland, lake-margin, and lake environments (*e.g.* Hay and Kyser, 2001). Previous studies of sediments from the Olduvai basin identified authigenic Mg-rich trioctahedral smectite (stevensite) and celadonite in the waxy claystones, along with other diagnostic minerals characteristic of hypersaline and alkaline conditions including carbonates, zeolites and K-feldspar (*e.g.* Hay, 1976; Hay and Kyser, 2001; Deocampo *et al.*, 2002). We focus in more detail on the microtextural and microgeochemical changes observed in the clay minerals from the lake-margin freshwater wetlands and interbedded waxy claystones, as well as on the waxy claystones of the central basin.

Mg uptake during smectite neoformation. Along the eastern lake margin, waxy claystones deposited during high lake levels are interbedded with earthy claystones deposited during low lake levels, when groundwater-fed freshwater wetlands developed (Ashley, 1996; Deocampo and Ashley, 1999; Ashley, 2000; Liutkus and Ashley, in press). By analogy with modern saline alkaline lakes, the formation of authigenic Mg-rich smectite in the waxy claystones was probably the result of elevated $H_4SiO_4^0$ and Mg^{2+} concentrations caused by the evapoconcentration of surface waters, the alkaline pH (~ 9–10), and precipitation of Ca carbonates and Na-rich zeolites (*e.g.* Tardy *et al.*, 1974; Gac *et al.*, 1977; Jones and Weir, 1983; Yuretich and Cerling, 1983; von Damm and Edmond, 1984; Jones, 1986; Darragi and Tardy, 1987; Banfield *et al.*, 1991b). In contrast, during deposition of the earthy claystones, the Na^+-HCO_3^--CO_3^{2-}-rich surface water in the freshwater wetlands probably had a relatively low pH (~7–7.5) resulting from elevated P_{CO_2} concentrations caused by the decay of organic matter, conditions that have been observed in modern groundwater-fed wetlands in the East African Rift (*e.g.* Deocampo and Ashley, 1999). These conditions probably promoted the preservation of siliceous components by decreasing the rate of silica dissolution and significant smectite neoformation was therefore unlikely.

The similarity in XRD patterns obtained from the <2 μm glycol-solvated clay aggregates from both the earthy and waxy claystone suggests that similar smectite components are present. The atypical d_{001} values of ~18 to 19.0 Å of smectite obtained from both the earthy and waxy claystones are larger than values obtained for smectite from the pyroclastic fan and alluvial plain (~17 Å), and are consistent with neoformation of a 'different' smectite component. Deocampo *et al.* (2002) concluded that similar XRD patterns obtained from the <0.2 μm fraction of earthy and waxy claystones represented an authigenic Mg-rich smectite component, which formed during periodic inundation of the freshwater wetlands by saline alkaline lake waters (Liutkus and Ashley, in press). Other studies have also documented similar large basal spacings ranging from ~17.6 to 18.4 Å for neoformed stevensite (Tettenhorst and Moore, 1978), especially for thin fiber-like crystals (Polyak and Güven, 2000), and in synthetic stevensite (Takahashi *et al.*, 1997).

The micro-textural, micro-structural and micro-geochemical data obtained in the present study provide the first direct observations of Mg-smectite neoformation in saline alkaline conditions. The TEM images and SAED patterns of smectite-altered volcanic glass particles in the earthy claystones indicates that smectite crystal morphologies, grain size, and degree of ordering are similar to those observed in the proximal pyroclastic fan and fluvial plain environments (compare Figures 7a and 7b with 5c and 5d). The lack of significant morphological or structural changes in smectite crystallites is consistent with the absence of significant smectite neoformation as a result of the relatively low pH and low Mg^{2+} and $H_4SiO_4^0$ activities predicted for the wetlands surface waters.

Similarly, the TEM images of smectite alteration of ash and pumice fragments in the waxy claystones generally show that the same feathery and anastomosing network of crystallites is present as occurs in the earthy

https://doi.org/10.1346/CCMN.2003.0510301 Published online by Cambridge University Press

claystones (compare Figure 7d with 7a). However, at higher magnification, textures observed in TEM images suggest that additional smectite alteration or neoformation is taking place. Smectite in waxy claystones from both the lake margin and lake basin, occurs as larger packets or 'quasi-crystals', composed of tens of thin individual crystallites (<5 nm) with many layer terminations and dislocations indicating highly disordered interfaces (Figure 7e). Lattice-fringe images show irregular and variable basal spacings between 11 and 14 Å (Figure 7e) and SAED patterns contain diffuse and smeared 00*l*, 0*kl* and *h*0*l* reflections (Figure 7f), consistent with disordered, turbostratic, smectite-rich material. The discontinuous 14 Å domains, observed only in smectite from waxy claystones, may be due to the presence of Mg hydroxyl groups in the interlayers, which are favored under high pH conditions (*e.g.* Carstea *et al.*, 1970). These domains may represent precursors to Mg-rich chlorite domains or mixed-layer smectite-chlorite intergrades described by Jones and Weir (1983) for modern Lake Abert sediments.

The composition of smectite from both the earthy and waxy claystones from the lake margin indicates that Mg uptake is occurring in both, but that the amount of Mg uptake is greater in the waxy claystones. Smectite compositions from the earthy claystones vary from very Al-rich compositions similar to those determined for the original detrital components from the proximal pyroclastic fan and fluvial plain, to moderately Mg-rich compositions (Figure 9). Similarly, the most Al-rich smectite compositions from the waxy claystones overlap original detrital smectite compositions, but extend to Mg contents greater than those observed in the earthy claystones (Figure 9). Smectite compositions from the lake basin are the most Mg rich of all (Figure 9).

To illustrate better the trends in smectite compositions, we plotted the variation of octahedral sheet trivalent (^{vi}Al+Fe(III)) content *vs.* Mg content of the smectite in Figure 10a (*e.g.* Paquet *et al.*, 1987). The composition of a fully occupied octahedral sheet (*e.g.* +12 charge) should fall along the line between the pure dioctahedral ((^{vi}Al+Fe(III)) = 4 c.p.f.u.) and trioctahedral (Mg = 6 c.p.f.u.) end-members. A compositional gap is thought to exist between the dioctahedral domain ^{vi}Al+Fe(III contents <2.6 c.p.f.u.; Weaver and Pollard (1973)), and the trioctahedral domain (Mg contents >3.66 c.p.f.u.; Foster (1960)).

The AEM spot analyses of smectite from the proximal pyroclastic fan and fluvial plain plot within the dioctahedral domain along a linear trend, shown by the field enclosed by the dashed line in Figure 10a. All data are offset from the ideal line due to the presence of site vacancies in the octahedral sheet and to a small amount of octahedral Mn and Ti, which are not accounted for in the diagram. These AEM-determined compositions compare favorably with the smectite composition obtained from a bulk-clay mineral separate (<2 μm) from a weathered tuff layer exposed in the western fluvial plain by Hay and Kyser (2001) (Figure 10a).

The variation in ^{vi}Al+Fe(III) content *vs.* Mg content of smectite from the lake-margin earthy and waxy claystones lie along the linear trend between the di- and trioctahedral end-members (Figure 10a). The most Al-rich smectite compositions plot within the dioctahedral domain and overlap compositions from the pyroclastic fan and fluvial plain. However, the majority of smectite analyses from the earthy claystones and most of the analyses from the waxy claystones fall within the 'compositional gap' between the di- and trioctahedral domains. These smectite compositions have total octahedral occupancies of up to 4.3 c.p.f.u. in the earthy claystones and up to 4.8 c.p.f.u. in the waxy claystones, indicating that excess octahedral cations are present relative to a dioctahedral end-member. The compositions of lake-basin smectites fall within the trioctahedral domain (Figure 10a), and are deficient in total octahedral cations relative to ideal trioctahedral smectite (5.4 c.p.f.u.) consistent with stevensite compositions.

These AEM-determined smectite compositions compare well with 'average' smectite compositions obtained on bulk clay separates (<2 μm) by Hay and Kyser (2001) and ultra-fine clay separates (<0.1 μm) by Deocampo *et al.* (2002) (Figure 10a). Although not differentiated in Figure 10a, the smectite spot analyses from a single earthy or waxy claystone sample are extremely heterogeneous and span the entire compositional range measured in each lithology. Thus, the variability in smectite compositions exhibited at the nm scale within one sample suggests that the progressive increase in the Mg content of smectite with distance from the freshwater wetlands towards the lake center, observed by Deocampo *et al.* (2002), may be fortuitous.

Jones and Weir (1983), Jones (1986) and Webster and Jones (1994) suggested that precipitation of authigenic Mg-rich smectite in saline alkaline lakes is facilitated by the presence of precursor dioctahedral 2:1 layer silicates, which act as substrates for neoformation. Banfield *et al.* (1991b) interpreted similar mixed di- and trioctahedral compositions obtained by AEM methods to result from the topotactic growth of Mg-rich smectite on original detrital Al-rich precursors during neoformation in Lake Abert, Oregon. Similarly, Çolak *et al.* (2000) suggested that the variable Mg/Al ratios in smectite from lacustrine borate deposits (Emet, Turkey) resulted from the overgrowth of Mg-rich trioctahedral smectite on original detrital dioctahedral smectite. Neoformed Mg-rich smectite with variable (^{vi}Al+Fe(III))/Mg ratios has also been described for hypersaline marine tidal flats in the Salina Ometepec, Baja, California (Hover *et al.*, 1999). Intermediate compositions obtained during experimental synthesis have also been interpreted to result from physical mixtures of discrete di- and trioctahedral components, with domain sizes as small as a few layers

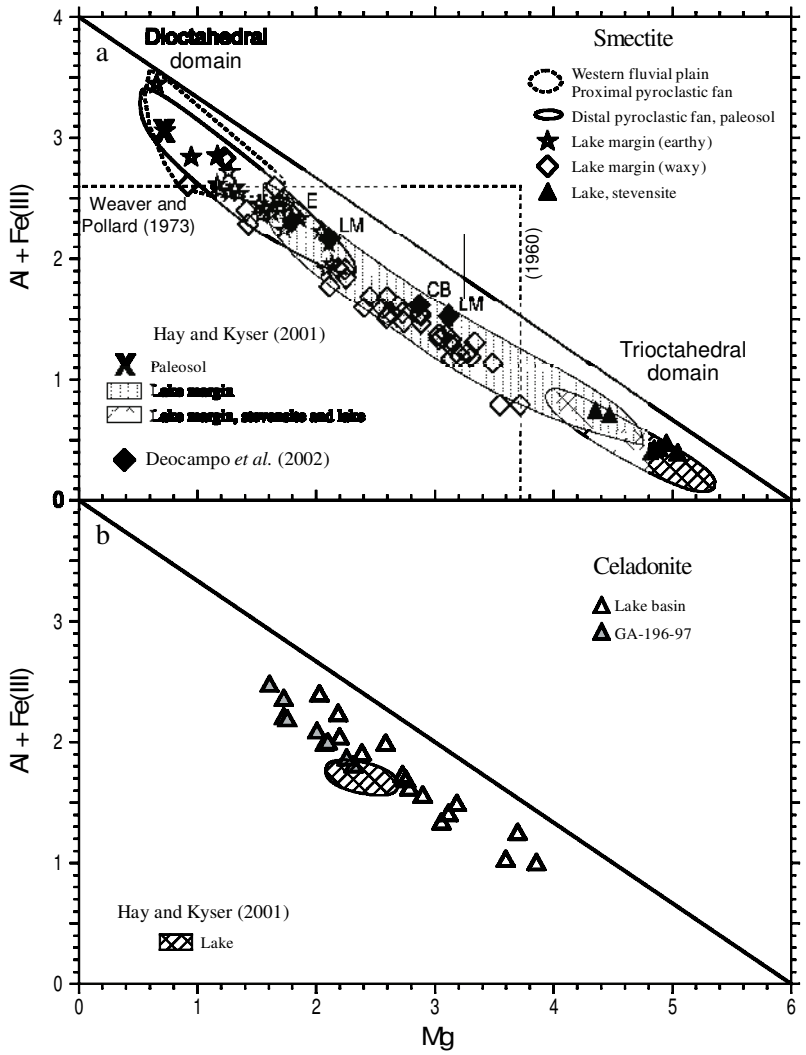

Figure 10. The variation in ^{vi}Al+Fe(III) *vs*. Mg in clay minerals from the Olduvai Basin. (a) Smectite compositions from the proximal pyroclastic fan and fluvial plain are enclosed within the dashed line and fall within the dioctahedral domain. Individual spot analyses of smectite from the earthy and waxy claystones from the lake margin basin extend between the di- and trioctahedral domains. Smectite compositions from the lake basin fall within the trioctahedral domain and are close to stevensite in composition. The smectite compositions obtained by Hay and Kyser (2001) (<2 μm bulk fraction) are enclosed in the shaded fields. The bulk compositions of smectite in an earthy claystone (EC) and waxy claystones (WC) obtained by Deocampo *et al.* (2002) (<0.2 μm bulk fraction) are shown by the solid squares. (b) Celadonite compositions in waxy claystones from the lake basin. The shaded triangles are analyses from sample GA-197-97, which contains the most dioctahedral compositions. Celadonite compositions obtained by Hay and Kyser (2001) are enclosed in the shaded field.

(or parts of layers) (*e.g.* Decarreau *et al.*, 1992; Huertas *et al.*, 2000).

We interpret the variable (^{vi}Al+Fe(III))/Mg compositions obtained in our study to result from mixtures of original dioctahedral detrital smectite and authigenic trioctahedral smectite within the area of analysis. The TEM images show that there are no significant textural or structural features that can be used to distinguish original detrital from authigenic smectite with the possible exception of the presence of larger 'quasi-crystals' and local domains of 14 Å in smectite from the waxy claystones. Therefore, AEM analyses obtained on such material must include mixtures of both detrital and authigenic smectite. We concur with the conclusions reached by Banfield *et al.* (1991b), and suggest that the observed heterogeneous compositions of smectite in the waxy claystones results from the topotactic overgrowth of an Mg-rich smectite component on an original detrital dioctahedral smectite. The process may include partial dissolution of the original detrital smectite followed by precipitation of Mg-rich smectite.

The relatively homogeneous, Mg-rich, ^{vi}Al- and Fe(III)-poor stevensite from the lake basin samples suggests nearly complete removal (dissolution) of the

https://doi.org/10.1346/CCMN.2003.0510301 Published online by Cambridge University Press

original detrital Al-rich smectite, and direct precipitation from alkaline lake waters occurred. The presence of diatom frustules or amorphous silica gels may have facilitated the Mg-smectite neoformation (Badaut and Rasacher, 1983; Banfield *et al*., 1991b).

Celadonite neoformation. Although the neoformation of celadonite in the waxy claystones of the Olduvai lake basin has been described by Hay and Kyser (2001), ours is the first study to document its formation at the microcrystalline scale. Our XRD and TEM data indicate that some waxy claystones from the lake margin and most waxy claystones from the lake basin contain a discrete 10 Å phase with dioctahedral celadonitic composition and textures consistent with neoformation. In the waxy claystones from the lake margin, the 10 Å phase makes up only a minor percentage of the total clay fraction and comprises small (<~30 nm diameter) and thin (<~10 nm thick) euhedral crystallites with pseudohexagonal boundaries (Figure 7g) and relatively straight and uniform 10 Å (001) lattice fringes (Figure 7i). The SAED patterns obtained on these crystallites contain discrete diffraction spots consistent with some coherency between layers (Figure 7h) and $1M_d$ polytypism (Figure 7j). The SAED patterns also include contributions from highly disordered smectite-like material within the area of the analyses.

The TEM images of waxy claystones containing only the 10 Å phase show that individual crystallites are larger (up to 50 nm), have distinct euhedral pseudohexagonal grain boundaries (Figure 7k), and thicker packet size (up to ~15 nm) (Figure 7m). The SAED patterns obtained on grain mounts contain sharp *hk*0 diffraction spots with hexanet symmetry (Figure 7l) and those obtained on ion-thinned samples contain sharp 00*l* and faint 0*kl* diffraction spots consistent with coherent crystals (Figure 7n). There is little evidence for the presence of disordered smectite-like material within the area of analysis. Thus, the microtextural and microstructural properties of celadonite from the lake basin appear to represent a more advanced stage of neoformation relative to that of the lake margin, and that nearly all of the precursor smectite has been completely replaced by authigenic celadonite.

The variation of (^{vi}Al+Fe(III)) content *vs*. Mg content of celadonite lie along a linear trend between the dioctahedral Al-rich (muscovite) and trioctahedral Mg-rich (phlogopite) end-members (Figure 10b). The analyses from sample GA-196-97, with total octahedral occupancies of 4.0–4.2 c.p.f.u., are nearly ideally dioctahedral (shaded triangles, Figure 10b). The analyses that plot at Mg contents >~2.2 c.p.f.u. have higher total octahedral occupancies of 4.2–4.6 c.p.f.u. and represent mixed di- and trioctahedral components are present. It is likely that these analyses reflect mixtures with Mg-rich smectite also present in those samples. The AEM of the most celadonitic (dioctahedral) material are similar to compositions reported for bulk-clay-mineral separates of celadonite by Hay and Kyser (2001).

The neoformation of 10 Å clay minerals in saline alkaline lake sediments has implications for environmental interpretations. Stoffers and Singer (1979) and Singer and Stoffers (1980) attributed the formation of a 10 Å illitic phase in intervals of the Pleistocene to Holocene sediments from Lake Mobuto Sese Seko (Abert) and Lake Manyara to be the result of an increase in the K^+/Na^+ ratio of the lake caused by the concomitant formation of analcime during periods of increased salinity in the lake basin. Similarly, Hay and Kyser (2001) suggested that celadonite neoformation in the Olduvai basin sediments occurred during conditions of higher salinity, which increased the K^+/Mg^{2+} activity ratio and pH relative to those that resulted in Mg-smectite formation. Thus, the occurrence of neoformed 10 Å clay in continental lake environments appears to represent the most saline lake conditions.

Progressive diagenetic reactions. The combined microtextural and geochemical data obtained on smectite from the lake margin and lake environments indicates that whereas the earthy claystones from the lake margin largely retain original detrital textures, the composition of smectite is modified by the neoformation of an Mg-rich component, probably during episodic inundation of the freshwater wetlands by saline alkaline lake waters (Liutkus and Ashley, in press). The clay mineral microtextures observed in the waxy claystones are different from those observed in the interbedded earthy claystones and indicate that more extensive replacement of original detrital dioctahedral smectite by neoformed smectite and celadonite has occurred in the alkaline lake waters. The replacement is most complete in the waxy claystones of the lake and smectite compositions approach end-member stevensite. Hay and Kyser (2001) estimate that 70% of the solutes necessary for stevensite are derived from the lake waters. The coexistence of Mg-rich smectite (stevensite) with Al-celadonite suggests that the Al may come, in part, from the dissolution of the original detrital Al-rich component of the smectite. The absence of the trioctahedral Mg-rich clay mineral kerolite, a common diagenetic clay mineral in other continental lake environments (*e.g*. Eberl *et al*., 1982; Khoury *et al*., 1982), suggests that lake water compositions were more saline and K rich (*e.g*. Jones, 1986).

The collective textural and geochemical data indicate that the progressive diagenetic reaction that takes place with increasing salinity and alkalinity at ambient temperature conditions in the Olduvai basin is: Al-rich dioctahedral smectite → Mg-rich trioctahedral stevensite ± celadonite → celadonite.

The TEM images of celadonite show textures consistent with neoformation via dissolution and precipitation processes.

https://doi.org/10.1346/CCMN.2003.0510301 Published online by Cambridge University Press

CONCLUSIONS

Our high-resolution study of clay mineralogy, textures, structures, and compositions in sediments from a transect across the paleo-sedimentary Olduvai basin indicates that the smectite-rich clay mineral assemblage records subtle differences in original depositional environments and post-depositional changes in pedogenic and diagenetic environments. In general, sediments from distal fluvial environments furthest from the lake, which were exposed only to pedogenic processes, contain dominantly dioctahedral Al-rich smectite. Sediments from the lake margin and lake basin, which were exposed to saline alkaline lake water, contain various proportions of Mg-rich trioctahedral smectite and dioctahedral celadonite.

In the more deeply weathered soils of the distal pyroclastic fan closer to the lake margin, the Al-rich dioctahedral compositions are retained, but repeated wetting and drying cycles probably caused the additional uptake of K into smectite interlayers, and the reorganization of some smectite layers to more ordered illite-like domains. Neoformation of additional Mg- and Fe(III)-rich smectite also occurs.

In the earthy claystones from the lake-margin freshwater-wetlands, the original textures, crystal morphology, and degree of ordering acquired by smectite during alteration of volcanic glass in the pedogenic (weathering) environment are largely retained. However, smectite compositions are modified as a result of neoformation of trioctahedral Mg-rich smectite (stevensite), probably during episodic inundation by saline-alkaline lake-waters.

In the waxy claystones from the lake margin and lake basin, relict volcanic glass alteration textures acquired in the pedogenic environment are still observed in some samples, though the smectite alteration appears as larger 'quasi-crystal' aggregates composed of many small individual crystallites stacked in disordered (turbostratic) arrangement. The Mg content varies widely, due to the presence of physical mixtures of original detrital Al-rich dioctahedral smectite and topotactic overgrowths of authigenic Mg-rich trioctahedral stevensite. Smectite from the lake basin is nearly pure stevensite, which indicates complete replacement (dissolution) of the original Al-rich smectite by authigenic (re-precipitated) Mg-rich stevensite.

Waxy claystones also contain authigenic 10 Å celadonite, the proportion of which varies from a few scattered fine-grained euhedral crystals within smectite-rich domains in lake-margin environments to massive intergrowths made up entirely of fine-grained euhedral celadonite crystals.

The collective mineralogical, textural and geochemical data indicate that under conditions of increasing salinity and alkalinity, the progressive alteration of detrital smectite to 10 Å celadonite proceeds according to the reaction:

Al-rich dioctahedral smectite →
Mg-rich trioctahedral stevensite ± celadonite →
celadonite.

Clay mineralogy and geochemistry determined at a basin-wide scale can be used to discriminate among the represented paleoenvironments. The spatial and temporal distribution of these paleoenvironments can be applied ultimately to the interpretation of changes in paleoclimatic conditions.

ACKNOWLEDGMENTS

Samples used in this study were collected under Tanzanian permits to the Olduvai Landscape Paleoanthropology Project (OLAPP). The principal investigators are R.J. Blumenschine (Rutgers, the State University of New Jersey), F.T. Masao (University Dar es Salaam, Tanzania) and C.R. Peters (University of Georgia). We would like to thank D. Deocampo, C. Swisher, A. Deino, R. Renaut and G. Mollel for discussions on the geology and A. Cushing, S. Copeland, J. Tactikos, J. Njau, J. Mosi, R. Mrema, A. Valence and G. Peters for assistance in the field. We greatly appreciate the hospitality of the Olduvai Museum Staff, O. Kileo, J. Paresso and G. Olle Moita. We are particularly grateful to R. Hay for his valuable insights into the stratigraphy of Olduvai and his generosity in discussing ideas, sharing data and commenting on an early version of this manuscript. The manuscript was much improved by the thoughtful reviews of R. Hay and R. Yuretich and editorial handling by D.C. Bain. The research was sponsored by NSF grants (Archaeology BNS 9000099 and SBR 961065) to R.J. Blumenschine and F.T. Masao, and (Geosciences 9903258) to G.M. Ashley and J.S. Delaney. Acknowledgement is also made to the Donors of the Petroleum Research Fund, administered by the American Chemical Society (PRF 36498-AC8) to V.C. Hover for support of this research. The STEM used in the study was acquired under NSF grant (Geosciences EAR 8708276).

REFERENCES

Ashley, G.M. (1996) Springs, pools, and adjacent wetlands, a newly recognized habitat, lowermost Bed II, Olduvai Gorge, Tanzania. *Geological Society of America Abstracts with Program*, **26**, 28.

Ashley, G.M. (2000) Geologists probe Hominid environments: Geological Society of America 1999 Presidential Address. *GSA Today*, **10**, 24–29.

Ashley, G.M. (2001) Orbital rhythms, monsoons, and playa lake response, Olduvai Basin, Equatorial East Africa at 1.85–1.75 Ma. *EOS, Transactions, American Geophysical Union, supplement, Abstracts*, **82(47)**, F759.

Ashley, G.M. and Driese, S.G. (2000) Paleopedology and paleohydrology of volcaniclastic paleosol: implications for Early Pleistocene paleoclimate record, Olduvai Gorge, Tanzania. *Journal of Sedimentary Research*, **70**, 1065–1080.

Ashley, G.M. and Hay, R.L. (2002) Sedimentation patterns in a Plio-Pleistocene volcaniclastic rift-platform basin, Olduvai Gorge, Tanzania. Pp. 107–122 in: *Sedimentation in Continental Rifts* (R.W. Renaut and G.M. Ashley editors). SEPM Special Publication, **73**. Society for Sedimentary Geology, Tulsa, Oklahoma.

Ashley, G.M. and Renaut, R.W. (2002) Rift Sedimentation. Pp. 3–10 in: *Sedimentation in Continental Rifts* (R.W.

Renaut and G.M. Ashley editors). SEPM Special Publication, **73**. Society for Sedimentary Geology, Tulsa, Oklahoma.

Badaut, D. and Risacher, F. (1983) Authigenic smectite on diatom frustules in Bolivian saline lakes. *Geochimica et Cosmochimica Acta*, **47**, 363–375.

Banfield, J.F. and Barker, W.W. (1998) Low-temperature alteration in tuffs from Yucca Mountain, Nevada. *Clays and Clay Minerals*, **46**, 27–37.

Banfield, J.F., Jones, B.F. and Veblen, D.R. (1991a) An AEM-STEM study of weathering and diagenesis, Abert Lake, Oregon: I. Weathering reactions in volcanics. *Geochimica et Cosmochimica Acta*, **55**, 2781–2793.

Banfield, J.F., Jones, B.F. and Veblen, D.R. (1991b) An AEM-STEM study of weathering and diagenesis, Abert Lake, Oregon: II. Diagenetic modification of the sedimentary assemblage. *Geochimica et Cosmochimica Acta*, **55**, 2795–2810.

Baxter Grubb, S.M., Peacor, D.R. and Jiang, W.-T. (1991) Transmission electron microscope observations of illite polytypism. *Clays and Clay Minerals*, **39**, 540–550.

Blumenschine, R.J. and Masao, F.T. (1991) Living sites at Olduvai Gorge, Tanzania? Preliminary landscape archaeology results in the basal Bed II lake margin zone. *Journal of Human Evolution*, **21**, 451–462.

Blumenschine, R.J. and Peters, C.R. (1998) Archaeological predictions for hominid land use in the paleo-Olduvai Basin, Tanzania, during lowermost Bed II times. *Journal of Human Evolution*, **34**, 565–607.

Brindley, G.W. (1955) Stevensite, a montmorillonite-type mineral showing mixed-layer characteristics. *American Mineralogist*, **40**, 239–247.

Carstea, D.D., Harward, M.E. and Knox, E.G. (1970) Formation and stability of hydroxy-Mg interlayers in phyllosilicates. *Clays and Clay Minerals*, **18**, 213–222.

Çolak, M., Helvaci, C. and Maggetti, M. (2000) Saponite from the Emet colmenite mines, Kütahya, Turkey. *Clays and Clay Minerals*, **48**, 409–423.

Darragi, F. and Tardy, Y. (1987) Authigenic trioctahedral smectites controlling pH, alkalinity, silica and magnesium concentrations in alkaline lakes. *Chemical Geology*, **63**, 59–72.

Decarreau, A., Grauby, O. and Petit, S. (1992) The actual distribution of octahedral cations in 2:1 clay minerals: Results from clay synthesis. *Applied Clay Science*, **7**, 147–167.

de la Fuente, S., Cuadros, J., Fiore, S. and Linares, J. (2000) Electron microscopy study of volcanic tuff alteration to illite-smectite under hydrothermal conditions. *Clays and Clay Minerals*, **48**, 339–350.

Deocampo, D.M. and Ashley, G.M. (1999) Siliceous island in a carbonate sea: modern and Pleistocene records of spring-fed wetlands in Ngorongoro Crater and Olduvai Gorge, Tanzania. *Journal of Sedimentary Research*, **69**, 974–979.

Deocampo, D.M., Blumenschine, R.J. and Ashley, G.M. (2002) Wetland diagenesis and traces of early Hominids, Olduvai Gorge, Tanzania. *Quaternary Research*, **57**, 271–281.

Dong, H. and Peacor, D.R. (1996) TEM observations of coherent stacking relations in smectite, I/S and illite of shales: Evidence for MacEwan crystallites and dominance of $2M_1$ polytypism. *Clays and Clay Minerals*, **44**, 257–275.

Drever, J.I. (1973) The preparation of oriented clay mineral specimens for X-ray diffraction analysis by a filter-membrane peel technique. *American Mineralogist*, **58**, 553–554.

Eberl, D.D., Jones, B.F. and Khoury, H.N. (1982) Mixed-layer kerolite/stevensite from the Amargosa Desert, Nevada. *Clays and Clay Minerals* **30**, 321–326.

Eberl, D.D., Środoń, J. and Northrop, H.R. (1986) Potassium fixation in smectite by wetting and drying. Pp. 296–326 in: *Geochemical Processes at Mineral Surfaces* (J.A. Davis and K.F. Hayes, editors). ACS Symposium Series, **323**. The American Chemical Society, Washington, D.C.

Faust, G.T. and Murata, K.J. (1953) Stevensite, redefined as a member of the montmorillonite group. *American Mineralogist*, **38**, 973–987.

Faust, G.T., Hathaway, J.C. and Millot, G. (1959) A restudy of stevensite and allied minerals. *American Mineralogist*, **44**, 342–370.

Fiore, S. (1993) The occurrences of smectite and illite in a pyroclastic deposit prior to weathering: Implication on the genesis of 2:1 clay minerals in volcanic soils. *Applied Clay Science*, **8**, 249–259.

Foster, M. (1960) Interpretation of the composition of trioctahedral micas. *US Geological Survey Professional Paper* **354-B,** 11–50.

Frostick, L.E., Renaut, R.W., Reid, I. and Tiercelin, J.-J. (1986) *Sedimentation in the African Rifts*. Special Publication **25**. Geological Society of London, 382 pp.

Gac, J.Y., Droubi, A., Fritz, B. and Tardy, Y. (1977) Geochemical behavior of silica and magnesium during the evaporation of waters in Chad. *Chemical Geology*, **19**, 215–228.

Garrels, R.M. and Mackenzie, F.T. (1967) Origin of the chemical compositions of some springs and lakes. Pp. 222–242 in: *Equilibrium Concepts in Natural Water Systems* (W. Stumm, editor). Advances in Chemistry Series, **67**. American Chemical Society, Washington, D.C.

Guthrie, G.D. and Veblen, D.R. (1990) Interpreting one dimensional high-resolution transmission electron micrographs of sheet silicates by computer simulation. *American Mineralogist*, **75**, 276–288.

Hay, R.L. (1970) Silicate reactions in three lithofacies of a semi-arid basin, Olduvai Gorge, Tanzania. Pp. 237–255 in: *The Fiftieth Anniversary Symposia: Mineralogy and Petrology of the Upper Mantle, Sulfides, and Geochemistry of Non-marine Evaporites* (B.A. Morgan, editor). Special Paper, **3**. Mineralogical Society of America, Washington, D.C.

Hay, R.L. (1976) *Geology of Olduvai Gorge, a Study of Sedimentation in a Semiarid Basin*. University of California, Berkeley, California, 203 pp.

Hay, R.L. (1989) Holocene carbonatite-nephelinite tephra deposits of Oldoinyo Lengai, Tanzania. *Journal of Volcanic Geothermal Research*, **37**, 77–91.

Hay, R.L. (1990) Olduvai Gorge; A case history in the interpretation of hominid paleoenvironments in East Africa. Pp. 23–37 in: *Establishment of a Geologic Framework for Paleoanthropology* (L.F. Laporte, editor). Special Paper, **242**. Geological Society of America, Boulder, Colorado.

Hay, R.L. and Kyser, T.K. (2001) Chemical sedimentology and paleoenvironmental history of Lake Olduvai, a Pleistocene lake in northern Tanzania. *Geological Society of America Bulletin,* **113**, 1505–1521.

Hover, V.C., Walter, L.M., Peacor, D.R. and Martini, A.M. (1999) Mg-smectite authigenesis in a marine evaporative environment, Salina Ometepec, Baja, California, *Clays and Clay Minerals*, **47**, 252–268.

Hover, V.C., Walter, L.M. and Peacor, D.R. (2002) K-uptake by modern estuarine sediments during early marine diagenesis, Mississippi delta plain, Louisiana. *Journal of Sedimentary Research*, **72**, 775–792.

Huertas, F.J., Caudros, J., Huertas, F. and Linares, J. (2000) Experimental study of the hydrothermal formation of smectite in the beidellite-saponite series. *American Journal of Science*, **300**, 504–527.

Jackson, M.L. (1969) *Soil Chemical Analysis–Advanced Course.*

Published by the author, Madison Wisconsin, 895 pp.
Jiang, W.-T., Peacor, D.R., Merriman, R.J. and Roberts, B. (1990) Transmission and analytical electron microscopic study of mixed-layer illite/smectite formed as an apparent replacement product of diagenetic illite. *Clays and Clay Minerals*, **38**, 449–468.
Jones, B.F. (1986) Clay mineral diagenesis in lacustrine sediments. Pp. 291–300 in: *Studies in Diagenesis* (F.A. Mumpton, editor). *US Geological Survey Bulletin*, **1578**.
Jones, B.F. and Weir, A.H. (1983) Clay minerals of Lake Abert, an alkaline, saline lake. *Clays and Clay Minerals*, **31**, 161–172.
Khoury, H.N., Eberl, D.D. and Jones, B.F. (1982) Origin of magnesium clays from the Amargosa Desert, Nevada. *Clays and Clay Minerals*, **30**, 327–336.
Kim, J.-W., Peacor, D.R., Tessier, D. and Elsass, F. (1995) A technique for maintaining texture and permanent expansion of smectite interlayers for TEM observations. *Clays and Clay Minerals*, **43** 51–57.
Kappelman, J. (1984) Plio-Pleistocene environments of Bed I and lower Bed II, Olduvai Gorge, Tanzania. *Palaeogeography, Palaeoclimatology, and Palaeoecology*, **48**, 171–196.
Kappelman, J. (1986) Plio-Pleistocene marine-continental correlation using habitat indicators from Olduvai Gorge, Tanzania. *Quaternary Research,* **25**, 141–149.
Laird, D.A. (1994) Evaluation of the structural formula and alkylammonium methods of determining layer charge. Pp. 79–103 in: *Layer Charge Characteristics of 2:1 Silicate Clay Minerals* (A.R. Mermut, editor). CMS Workshop Lectures, **6**. Clay Minerals Society, Boulder, Colorado.
Leakey, L.S.B. (1965) *Olduvai Gorge: 1951–1961. Vol. I.* Cambridge University Press, Cambridge, UK.
Leakey, M.D. (1971) *Olduvai Gorge: Excavations in Beds I and II. 1960–1963*, Cambridge University Press, UK, 309 pp.
Liutkus, C.M. and Ashley, G.M. (2003) Sedimentology and stratigraphy of and ancient freshwater lake-margin wetland, Olduvai Gorge, Tanzania. *Journal of Sedimentary Research* (in press).
Moore, D.M. and Reynolds, R.C. (1997) *X-ray Diffraction and the Identification and Analysis of Clay minerals*. Oxford University Press, Oxford, UK, 378 pp.
Odin, G.S. (1988) *Green Marine Clays.* Elsevier, Amsterdam, 445 pp.
Paquet, H., Duplay, J., Valeron-Blanc, M.-M. and Millot, G. (1987) Octahedral compositions of individual particles in smectite-palygorskite and smectite-sepiolite assemblages. Pp. 73–77 in: *Proceedings of the International Clay Conference, Denver, 1985* (L.G. Schultz, H. van Olphen and F.A. Mumpton, editors). The Clay Minerals Society, Bloomington, Indiana.
Peacor, D.R. (1992a) Diagenesis and low grade metamorphism of shales and slates. Pp. 335–380 in: *Minerals and Reactions at the Atomic Scale: Transmission Electron Microscopy* (P.R. Buseck, editor). Reviews in Mineralogy, **27**. Mineralogical Society of America, Washington, D.C.
Peacor, D.R. (1992b) Analytical electron microscopy: X-ray analysis. Pp. 113–140 in: *Minerals and Reactions at the Atomic Scale: Transmission Electron Microscopy* (P.R. Buseck, editor). Reviews in Mineralogy, **27**. Mineralogical Society of America, Washington, D.C.
Polyak, V.G. and Güven, N. (2000) Authigenesis of trioctahedral smectite in magnesium-rich carbonate speleothems in Carlsbad Cavern and other caves of the Guadalupe Mountains, New Mexico. *Clays and Clay Minerals*, **48**, 317–321.
Peters, C.R. and Blumenschine, R.J. (1995) Landscape perspectives on possible land use patterns for early hominids in the Olduvai Basin. *Journal of Human Evolution*, **29**, 321–362.
Reading, H. (1996) *Sedimentary Environments: Processes, Facies and Stratigraphy*, 3rd edition. Blackwell Science, UK 688 pp.
Reynolds, R.C., Jr (1980) Interstratified clay minerals. Pp. 249–303 in: *Crystal Structures of Clay Minerals and their X-ray Identification* (G.W. Brindley, and G. Brown, editors). Monograph, **5**, The Mineralogical Society, London.
Seifert, F. (1968) X-ray powder data for Mg-Al celadonite (leucophyillite) from Barcza, Poland. *Contributions to Mineralogy and Petrology*, **19**, 93–96.
Singer, A. (1980) The paleoclimatic interpretation of clay minerals in soils and weathering profiles. *Earth-Science Reviews*, **15**, 303–327.
Singer, A. (1984) The paleoclimatic interpretation of clay minerals in sediments–a review. *Earth-Science Reviews*, **21**, 251–293.
Singer, A. and Stoffers, P. (1980) Clay mineral diagenesis in two East African lake sediments. *Clay Minerals*, **15**, 291–307.
Środoń, J., Morgan, D.J., Eslinger, E.V., Eberl, D.D. and Karlinger, M.F. (1986) Chemistry of illite/smectite and end-member illite. *Clays and Clay Minerals*, **34**, 368–378.
Stoffers, P. and Singer, A. (1979) Clay minerals in Lake Mobuto Sese Seko (Lake Albert)–Their diagenetic changes as indicators of the paleoclimate. *Geologische Rundschau*, **68**, 1009–1024.
Takahashi, N., Tanaka, M., Satoh, T., Endo, T. and Shimada, M. (1997) Study of synthetic clay minerals. Part IV: synthesis of microcrystalline stevensite from hydromagnesite and sodium silicate. *Microporous Materials*, **9**, 35–42.
Tardy, Y., Cheverry, C. and Fritz, B. (1974) Néoformation d'une argile magnésienne dan les dépressions interdunaires du lac Tchad: Application aux domaines de stabilité des phyllosilicates alumineaux mangésiens et ferriéres. *Comptes Rendu Academy Science français, Paris Serial* C, **278**, 1999–2002.
Tazaki, K., Fyfe, W.S. and van der Gaast, S.J. (1989) Growth of clay minerals in natural and synthetic glasses. *Clays and Clay Minerals*, **37**, 348–354.
Tettenhorst, R. and Moore, G.E., Jr (1978) Stevensite oolites from the Green River Formation of central Utah. *Journal of Sedimentary Petrology*, **48**, 587–594.
Yuretich, R.F. and Cerling, T.E. (1983) Hydrogeochemistry of Lake Turkana, Kenya: mass balance and mineral equilibria in an alkaline lake. *Geochimica et Cosmochimica Acta*, **47**, 1099–1109.
van der Pluijm, B.A., Lee, J.H. and Peacor, D.R. (1988) Analytical electron microscopy and the problem of potassium diffusion. *Clays and Clay Minerals*, **36**, 498–504.
von Damm, K.L. and Edmond, J.M. (1984) Reverse weathering in the closed-basin lakes of the Ethiopian Rift. *American Journal of Science*, **284**, 835–862.
Warren, E.A. and Ransom, B. (1992) The influence of analytical error upon the interpretation of chemical variations in clay minerals: *Clays and Clay Minerals*, **27**, 193–209.
Weaver, C.D. and Pollard, L.D. (1973) *The Chemistry of Clay Minerals.* Developments in Sedimentology **15**. Elsevier Scientific Publishing Co., Amsterdam, 213 pp.
Webster, D.M. and Jones, B.F. (1994) Paleoenvironmental implications of lacustrine clay minerals from the Double Lakes Formation, southern high plains, Texas. Pp. 159–172 in: *Sedimentology and Geochemistry of Modern and Ancient Saline Lakes* (R.W. Renaut and W.M. Last, editors). SEPM Special Publication, **50**. Society for Sedimentary Geology, Tulsa, Oklahoma.

(*Received 26 June 2002; revised 3 January 2003; Ms. 672*)